

ABSORPTION SYSTEMS IN THE SPECTRA OF SIXTY-SIX $Z \gtrsim 4$ QUASARSCÉLINE PÉROUX¹

Institute of Astronomy, Madingley Road, Cambridge CB3 OHA, UK

LISA J. STORRIE-LOMBARDI

SIRTF Science Center, California Institute of Technology, MS 100-22, Pasadena CA 91125, USA

RICHARD G. MCMAHON, MIKE IRWIN

Institute of Astronomy, Madingley Road, Cambridge CB3 OHA, UK

AND

ISOBEL M. HOOK

Institute for Astronomy, Royal Observatory, Blackford Hill, Edinburgh EH9 3HJ, UK

Accepted by the Astronomical Journal

ABSTRACT

We present high signal-to-noise, ~ 5 Å resolution (FWHM) spectra of 66 $z \gtrsim 4$ bright quasars obtained with the 4 m Cerro Tololo Inter-American Observatory and 4.2 m William Hershel telescopes. The primary goal of these observations was to undertake a new survey for intervening absorption systems detected in the spectra of background quasars. We look for both Lyman-limit systems (column densities $N_{HI} \geq 1.6 \times 10^{17}$ atoms cm $^{-2}$) and damped Ly α systems (column densities $N_{HI} \geq 2 \times 10^{20}$ atoms cm $^{-2}$). This work resulted in the discovery of 49 Lyman-limit systems, 15 of which are within 3000 km s $^{-1}$ of the quasar emission and thus might be associated with the quasar itself, 26 new damped Ly α absorption candidates, 15 of which have $z > 3.5$ and numerous metal absorption systems. In addition ten of the quasars presented here exhibit intrinsic broad absorption lines.

Subject headings: galaxies: evolution—galaxies: high-redshift—line: identification—quasars: absorption lines—quasars: general—surveys

1. INTRODUCTION

Because they are extremely luminous, quasars are among the youngest objects observed in the Universe, and have now been detected out to redshifts of $z \sim 5.8$ (Fan et al. 2000). Observing quasars at such high redshifts gives us direct indications of the ionization state of the early Universe. Indeed the lack of an observed Gunn-Peterson effect (Gunn & Peterson 1965) indicates that the Universe is already ionized at these early epochs.

In addition to being important observations in their own right, spectroscopic studies of quasars allow the detection of much fainter systems, observed in absorption in the quasar spectra. There are two main classes of quasar absorption lines: the metal systems, such as CIV or MgII, and the more numerous hydrogen lines. The latter are subdivided into three different groups according to their neutral hydrogen column densities. The Lyman- α forest absorbers have column densities $10^{12} - 1.6 \times 10^{17}$ atoms cm $^{-2}$. The Lyman-limit systems (hereafter LLS) have $N_{HI} \geq 1.6 \times 10^{17}$ atoms cm $^{-2}$ and the damped Lyman- α systems (hereafter DLA) are a subset of the LLS with $N_{HI} \geq 2 \times 10^{20}$ atoms cm $^{-2}$. They thus probe media with different column densities spanning the range from voids through to halos and disks of both dwarf and normal (proto)galaxies. The morphology of DLAs in particular is still open to debate. The hypotheses put forward range through large disk systems (Prochaska & Wolfe 1998), low surface brightness galaxies (Jimenez et al. 1999) and dwarf galaxies (Matteucci et al. 1997). Although the exact nature of the quasar absorbers is not known, they form a

sample of systems unbiased as regards luminosity, specific morphology, metallicity, or emission line strength, thus enabling studies of metallicity and HI evolution over a large redshift range.

The primary goal of our spectroscopic campaign is to obtain a statistically significant number of high-redshift absorbers to answer the questions raised by the apparent deficit of high column density systems at such redshifts (Storrie-Lombardi et al. 1996a; Storrie-Lombardi & Wolfe 2000). In particular we aim to study in more detail the evolution with redshift of the column density distribution, number density, and comoving mass density of high column density HI absorption systems. The latter has been quite controversial in the last few years. Lanzetta et al. 1995 found that Ω_{DLA} at $z \sim 3.5$ is twice the value at $z \sim 2$, implying a larger star formation rate than indicated by metallicity studies. This created the so-called “cosmic G-dwarf problem”. Storrie-Lombardi et al. 1996b used new data to show that Ω_{DLA} decreases at high-redshift thus solving the “cosmic G-dwarf problem”. The work of Storrie-Lombardi & Wolfe 2000 confirmed such results by using a compilation of data gathered from the literature together with new spectroscopic observations. The aim of our new survey for quasar absorbers is to better understand the high-redshift end of the mass density of neutral hydrogen by significantly improving the statistics at $z \gtrsim 3.5$. At low-redshift, recent studies by Rao & Turnshek 2000 show that Ω_{DLA} might be higher than first expected. Their analysis is based on HST observations of quasars with known MgII systems (MgII always

¹e-mail: celine@ast.cam.ac.uk

being associated with DLA systems, the reverse not being true). Nevertheless it should be emphasized, as the authors themselves pointed at, that the analysis is based on a relatively small number of systems. At all redshifts such measurements can be used to constrain the most recent semi-analytical models of galaxy formation (Kauffmann & Haehnelt 2000 and Somerville et al. 2000, which build on models originally presented by Kauffmann, White, & Guiderdoni 1993 and Cole et al. 1994). Several fundamental questions remain including locating the epoch of DLAs assembly, clarifying the the relationship between Lyman limit systems and damped absorbers, measuring the total amount of neutral hydrogen contained in quasar absorbers and studying how this varies with redshift. We will discuss the impact of our new survey on these issues in more detail in future papers currently in preparation (Peroux et al. 2000).

Any survey for quasar absorbers begins with a search for bright quasars and so constitutes an ambitious observational program. We observed sixty-six $z \gtrsim 4$ quasars discovered by various groups (Storrie-Lombardi et al. 2000, Fan et al. 1999, Warren, Hewett & Osmer 1991, Kennefick et al. 1995a, Storrie-Lombardi et al. 1996a, Zickgraf et al. 1997, Kennefick et al. 1995b, Henry et al. 1994, Hook et al. in preparation and Hall et al. 1996) almost all of which have not been previously studied at such resolution (≈ 5 Å) and signal-to-noise (ranging from 10–30). We obtained optical spectra at the 4.2 m William Herschel Telescope for the northern quasars and at the 4 m Cerro Tololo Inter-American Observatory for the southern objects. More information about $z \gtrsim 4$ quasars is available at the following URL: <http://www.ast.cam.ac.uk/~quasars>.

This paper is organized as follows. In §2 we provide the details of the set-up for each observational run and in §3 describe the data reduction and present the quasar spectra. Accurate quasar redshift and magnitude measurements are given in §4. The surveys for Lyman-limit systems and damped Ly- α absorbers are presented in §5 and §6, respectively. Provisional interpretation of metal absorption features are summarized in §7. Notes on individual objects are provided in §8 and conclusions are presented in section §9.

2. OBSERVATIONS

All the new observations were carried out during two observing runs at the 4.2 m William Herschel telescope (WHT) of the Isaac Newton Group of telescopes in the Canary Islands and two observing runs at the Blanco 4 m telescope at the Cerro Tololo Inter-American Observatory (CTIO) in Chile. High signal-to-noise optical spectrophotometry was obtained covering approximately 3500 Å to 9000 Å, the exact range depending on which instrument was used for the observations. A journal of the observations is presented in Table 1.

Thirty-one (including a $z=1.90$ quasar PSS J0052+2405) quasars were observed at the WHT during 1998 September 22-24 and 1999 March 18-19. The integration times were typically 1800 – 3600 seconds. We used the ISIS double-spectrograph which consists of two independant arms fed via a dichroic allowing for blue

and red observations to be carried out simultaneously. Gratings with 158 lines mm⁻¹ and a dichroic to split the light at ~ 5700 Å were used. This gives a dispersion of 2.89 Å pixel⁻¹ in the red arm and 1.62 Å pixel⁻¹ in the blue. The gratings were arranged so that the blue part of the spectrum was centered on 4500 Å while the red was centered on 7000 Å. On the blue arm a thinned coated English Electric Valve (EEV) 2148 × 4200 CCD with 13.5 μm pixels was used as detector. On the red arm a thinned coated Tektronix 1124 × 1124 CCD with 24 μm pixels was used. All the narrow-slit observations were taken with a slit width of 1.2 – 1.5 arcsec while the wide-slit observations were carried out with a slit width of 5 – 7 arcsec. Blind-offsetting from bright ~ 15 – 17^{th} magnitude stellar fiducials was used to position the quasars in the slit partly to save acquisition time and partly because the majority of the quasars were not visible using the blue sensitive TV acquisition system. Readout time was reduced by windowing the CCDs in the spatial direction.

Thirty-five quasars were observed at CTIO during 1998 October 14 – 16, and 1999 October 9 – 12. The typical exposure time was 3600 seconds for the brighter objects (R ~ 18 – 19^{th} mag) but substantially longer times were used for the fainter Sloan Digital Sky Survey quasars. We used the R-C spectrograph with the 316 lines mm⁻¹ grating, centered at 6050 Å and covering the range 3000Å–9100Å. This set-up resulted in a dispersion of 1.98 Å pixel⁻¹. The detector used was a Loral 3072 × 1024 CCD detector. The narrow and wide slit observations were taken with 1 – 1.5 arcsec and 5 arcsec widths, respectively. Because of the substantial wavelength coverage available with this set-up we used a WG345 blocking filter (with 50 % transmission at 3450 Å) to minimize the second order contamination from the standard stars above 7000 Å. The contamination is negligible for the quasars as most have no flux below 4500 Å but affects the standard stars that have substantial flux at 3500 Å. Appropriate measures, as discussed in the data reduction section, have been taken so that this set-up does not modify the flux calibration at the red end of the spectra. Using two instrumental set-ups in order to completely remove the second order contamination problem would have resulted in a 60–80 % increase in the required observing time.

The observations of SDSS J0338+0022 were taken at the Keck Observatory with the Low Resolution Imaging Spectrometer (LRIS). The observational details are given in Songaila et al. (1999).

3. DATA REDUCTION

The data reduction was undertaken using the IRAF¹ software package. Because the bias frames for each nights were so similar, a master ‘zero’ frame for each run was created using the IMCOMBINE routine. The data were overscan corrected, zero corrected, and trimmed using CCD-PROC. Similarly a single flat-field frame was produced by taking the median of the Tungsten flats. The overall background variation across this frame was removed to produce an image to correct for the pixel-to-pixel sensitivity variation of the data. The task APALL was used to extract 1-D multi-spectra from the 2-D frames. The routine esti-

¹IRAF is distributed by the National Optical Astronomy Observatories, which are operated by the Association of Universities for Research in Astronomy, Inc., under cooperative agreement with the National Science Foundation.

mates the sky level by model fitting over specified regions on either side of the spectrum.

The WHT data were wavelength calibrated using CuAr and CuNe arcs and monitored using night sky lines. Arcs were taken at each object position for wavelength calibrating the CTIO data. We used solely the sky lines to wavelength calibrate the Keck data. The spectra were flux calibrated using observations taken of spectrophotometric standards. B-stars free of strong features in the red were observed in order to remove the effects of atmospheric absorption in the red-arm WHT spectra and the CTIO spectra (e.g. O₂ A band at 7600 Å). The atmospheric absorption features seen in the B-star spectrum were isolated by interpolating between values on either side of the feature. The original B-star spectrum was then divided by this atmospheric-free spectrum to create an atmospheric correction spectrum. Finally the object spectra were divided by the scaled correction spectrum. In the case of ISIS data the red and blue ends of the spectra were then joined using SCOMBINE. In all cases if a wide-slit observation was made (see Table 1), it was used to correct the absolute flux levels for slit losses.

As mentioned in §2, the quasar spectra observed using the R-C spectrograph at CTIO suffered a gradual flux decrement in the red end calibration due to the inclusion of the second order flux from the standard stars. In order to correct for this effect, spectra of standard stars were taken with two different blocking filters (3450 Å and 5000 Å). The effect of the filter at wavelengths above 8000 Å could thus be determined and a correction applied accordingly to the quasar spectra. In addition a quasar previously observed with the ISIS double-spectrograph on WHT was re-observed at CTIO and corrected as explained above. Comparing the two spectra reveals no significant difference and provides a successful double check on the method. In any case the flux calibration of the red end of the spectra is relatively unimportant for the work undertaken here, namely the search of quasar absorbers blueward of the Ly- α emission.

The resulting spectra have a signal-to-noise ratio ranging from $\approx 10 - 30$ at 7000 Å. They are shown in Figure 1 with arbitrary flux scales. Ten of the quasars presented here exhibit intrinsic broad absorption lines (BAL). The feature in all of the CTIO spectra at 8900 Å is due to bad columns. In the 1999 run, the objects were moved along the slit between exposures so the effects of the bad columns were spread over a slightly wider region of the spectrum.

4. REDSHIFT AND MAGNITUDE MEASUREMENTS

In order to measure the redshifts, Gaussians were fit, if possible, to N V (rest wavelength 1240.13 Å), O I (1304.46 Å), Si IV + O IV] (1400.0 Å) and C IV (1549.1 Å) emission lines. The redshift for each line was determined from the central wavelength ($z = \lambda_{\text{observed}}/\lambda_{\text{emitted}} - 1$). Ly α (rest wavelength 1215.67 Å) is almost 50 % absorbed by the Ly α forest, so that the blue edge of the emission line has been used for redshift determination whenever possible. Some lines were impossible to fit and made the redshift determination difficult, especially in the case of the BALs. The redshift of each emission line, their average and the 1σ error are shown in Table 2. This error is representative of the error in the fit, in wavelength calibration (estimated to be

around 0.1 Å) and in the fact that the various species are coming from different physical regions of the quasar. In practice, this latter effect is probably the dominant source of differences in the emission line redshifts.

To provide an internal check on our redshift determinations we produced a median composite quasar spectrum. Each non-BAL spectrum with enough wavelength coverage was corrected to the rest-frame and scaled such that the median of the flux in a region free from emission lines (1420-1470 Å) is unity. The spectra were then rebinned into fixed 0.5 Å bins (i.e. similar to the resolution in the observed frame) and the median of the flux in each bin was calculated to produce the spectrum in Figure 2. Measuring the wavelength of the emission lines of the median composite spectrum provides an estimate of any systematic bias in the redshift measurements which in our case proves to be about $z=0.001$ (see last row of Table 2) and allows any shift in quasar redshifts to be checked by cross-correlation.

Table 3 summarizes the photometric and spectroscopic magnitudes for each object. The photometric magnitudes were measured from the UKST and POSS1 plates scanned using the APM facility. The spectroscopic magnitudes are derived from the spectra themselves using the IRAF task CALCPHOT and the “R59” (R) or “R63” (OR) filter curves for the quasars magnitudes from the UKST survey and the “e” filter curve for quasar magnitudes from POSS1 survey. These transmission curves are shown on Figure 3 overplotted on the $z=4.172$ BR J0529–3552 quasar spectrum. The error on the spectroscopic measurements is estimated to be $+/- 0.1$ mag and the error on the APM R magnitude is $+/- 0.25$ mag.

5. LYMAN-LIMIT SYSTEMS

5.1. Background

Lyman-limit systems (LLS) are absorption systems with hydrogen column densities $N_{HI} \geq 1.6 \times 10^{17}$ atoms cm⁻². They are defined by a sharp break (due to absorption of photons capable of ionizing HI) shortward of 912 Å. At $z < 1$, LLS are probably associated with galactic halos (Steidel, Dickinson & Persson 1994).

Because the search for absorption systems in quasar spectra is not biased towards luminous intervening objects, our data constitute a complementary way to the more traditional emission observations to probe galaxy evolution. The observed number density of LLSs per unit redshift can, for example, be directly compared with models of structure formation (i.e. Abel & Mo 1998). “Grey” LLS provide some of the best candidates for measurement of the primordial abundance of deuterium (Molaro et al. 1999, Levshakov et al. 2000 and references herein). Subsequent papers will make use of this new sample of LLS to constrain their space density, especially at $z \geq 2.4$ where we now have significantly more data than in previous surveys (e.g. Sargent, Steidel, & Boksenberg 1989; Lanzetta et al. 1991; Storrie-Lombardi et al. 1994; Stengler-Larrea et al. 1995).

5.2. LLS detection

The LLS were identified using an automated technique which determines the ratio (f_+/f_-) of the median of fluxes over 50 Å (rest frame) wide bins slid along the spectrum

(see Schneider et al. 1993 for details on this method). The minimum ratio corresponds to a potential LLS detection and the redshift is calculated from the corresponding wavelength. Two examples of the ratio versus LLS redshift plots are shown in Figure 4, one for a detection and the other for a non-detection. The optical depth is expressed as the logarithm of the ratio previously defined: $\tau_{LLS} = -\ln(f_+/f_-)$. In some cases, only a fraction of the radiation is absorbed forming a step in the quasar spectra which does not reach zero flux level. These so-called “grey” systems are only taken into account if they have an optical depth, $\tau > 1$. The redshifts and optical depths of the LLS detected in our sample of quasars are summarized in Table 4, together with the minimum and maximum redshift over which a LLS *could* have been detected. The minimum redshift corresponds to the smallest wavelength in the spectrum and the maximum redshift is 3000 km s^{-1} blueward of the quasar emission redshift. The actual redshift path surveyed is usually limited by the detection of the first Lyman-limit absorber, blueward of which there is either no residual flux or insufficient signal-to-noise to detect further LLSs. The analysis results in the detection of 49 LLS, 15 of which are within 3000 km s^{-1} of the quasar emission and thus might be associated with the quasar itself. In some cases, metal absorption features are also observed at the redshift of the LLS.

6. DAMPED LYMAN-ALPHA CANDIDATES

6.1. Background

Damped Lyman-alpha systems have, by definition (Wolfe et al. 1986), a rest-frame equivalent width $W \geq 10 \text{ \AA}$ corresponding to $N_{HI} \geq 2 \times 10^{20} \text{ atoms cm}^{-2}$. At low redshift such high HI column densities are found predominantly in gas rich systems such as the disks of spiral galaxies. Kinematic studies (such as Prochaska & Wolfe 1998 and Ledoux et al. 1998) and metallicity analyses (such as Pettini et al. 1997 and Prochaska & Wolfe 2000) indicate that DLAs at high-redshift might be the progenitors of present day galaxies. Detecting these systems beyond $z \geq 4$ provides observational information about the early stages of galaxy evolution.

DLAs are rare and to find them requires probing many quasar lines of sight. Figure 5 shows the cumulative number of lines of sight along which a DLA *could* have been detected at the 5σ confidence level. This survey sensitivity, $g(z)$, is compared with those of previous DLA surveys to show that our new observations more than double the redshift path searched for DLAs at $z \gtrsim 3.5$. Although DLAs have a low number density per unit redshift compared with lower column density systems, they are thought to contain most of the neutral hydrogen mass at $z < 3$. In a subsequent paper (Peroux et al. in preparation), we will discuss how this new survey impacts upon measurement of the comoving mass density of neutral gas at high redshift, its implications for the formation epoch of DLA and for the rate of evolution of gas into star.

6.2. DLA Detection

To select DLA candidates we have used the detection algorithm following the method developed by Lanzetta et al.

(1991), supplemented by a visual search. This has previously been applied to other samples of $z > 4$ quasars in Storrie-Lombardi et al. (1996a) and Storrie-Lombardi & Wolfe (2000). We used the same method for fitting the quasar continua as described in those papers. The spectra were analyzed from 3000 km s^{-1} blueward of the emission line (to avoid lines possibly associated with the quasar) towards shorter wavelengths. The analysis was stopped when the signal-to-noise ratio became too low to detect a Ly α line with rest equivalent width $\geq 5 \text{ \AA}$ at the 5σ level (corresponding to z_{min} in Table 5). This point was typically caused by the incidence of a Lyman limit system. We measured the equivalent widths of all the candidates with rest equivalent widths greater than 5 \AA and estimated their N_{HI} column densities from the linear part of the curve of growth. Previous experience has shown that the column density estimates derived using this method are in good agreement with measurements done on higher resolution data (compare Storrie-Lombardi et al. (1996c) and Storrie-Lombardi & Wolfe (2000)). The results are listed in Table 5. The candidates with rest equivalent widths in the range $5 - 10 \text{ \AA}$ at $z \sim 4$ are listed in the table for completion although they are unlikely to be damped.

Figure 6 shows two examples (BR J0006–6208 and BR J0307–4945) of the output of the algorithm we use to detect DLA candidates. The highest-redshift ($z=4.46$) DLA system currently known is detected in the spectrum of quasar BR J0307–4945 (Figure 7). It has many associated metal lines which have been studied in detail with higher-resolution observations undertaken with the UVES spectrograph (Dessauges-Zavadsky et al. 2000).

6.3. Metal Lines in the DLAs

Absorption features redward of the Ly- α quasar emission line were selected using an automated algorithm ² developed by Bob Carswell. The code systematically detects lines with equivalent width $W \geq 0.1 \text{ \AA}$. Gaussians were fitted to the lines in order to measure their redshifts and equivalent widths. Some of these lines were identified as low-ionization states of metals in association with DLA candidates. In some cases Ly- β was observed blueward of the DLA candidate. All the metal lines associated with DLA candidates are listed in Table 5.

7. METAL SYSTEMS

The observed equivalent width and wavelength of every absorption line detected redward of the quasar Lyman- α emission were measured using the algorithm described in section §6.3 above. The features which were not associated with a DLA or LLS were identified using the line list in Table 6. Most of the detected MgII systems also show associated Fe II absorption. This survey resulted in the detection of 80 new CIV systems ($3.0 \lesssim z \lesssim 4.5$) and 48 new MgII systems ($1.3 \lesssim z \lesssim 2.2$). The results are summarized in Table 7.

8. NOTES ON INDIVIDUAL OBJECTS

1. PSS J0003+2730 ($z=4.240$): This quasar has two weak Ly α absorbers at $z=3.51$ and 3.89 . Neither has an estimated column density greater than $10^{20.3} \text{ atoms cm}^{-2}$, but metal lines associated with both absorbers have been detected.

²see the following URL for more details: <http://www.ast.cam.ac.uk/~rfc/rdgen.html>

2. BR J0006–6208 (z=4.455): This quasar has weak emission lines but a rich absorption spectrum. There are four candidate damped absorbers at z=2.97, 3.20, 3.78 and 4.14. The highest redshift is a weak candidate but the other three all have high estimated column densities. All the candidates have at least one associated metal absorption line. In addition, there is a MgII absorption system at z=1.958.
3. BR J0030–5129 (z=4.174): This quasar has one candidate damped absorber at z=2.45 with three associated Fe II lines.
4. PSS J0034+1639 (z=4.293): This quasar has two damped Ly α candidate absorbers. The first is at z=3.75 and the estimated column density of log $N_{\text{HI}} = 20.2$ falls just below the formal definition of DLAs. Associated Si II and C IV metal lines are detected. The second damped system is at z=4.26 which is within 3000 km s $^{-1}$ of the emission redshift of the quasar (z=4.293) so it will not be included as an intervening absorber in the statistical samples used in determining the neutral gas mass. However it is of interest because this is the first damped system detected at a redshift greater than 4 with a column density log $N_{\text{HI}} > 21$. We estimate the column density for this system at log $N_{\text{HI}} = 21.1$ and detected associated metals lines of Si II, O I, C II, Si IV, C IV, and Fe II in the range z=4.252–4.282.
5. SDSS J0035+0040 (z=4.747): We detect no damped Ly α candidates in this spectrum. This is one of the lower signal-to-noise spectra in our sample due to the faintness of the quasar ($R=21.3$) but we would have been able to detect a DLA with a column density log $N_{\text{HI}} \geq 20.3$ over the redshift range $3.309 < z < 4.690$.
6. PSS J0052+2405 (z=1.90): This is a broad absorption lines quasar at z=1.9. We observed it because the coordinates were originally in the list of PSS $z > 4$ quasars available at their www site³. It has since been removed from that list.
7. Q J0054–2742 (z=4.464): This quasar exhibits broad absorption lines. The spectrum is not used in our absorption line survey.
8. PSS J0106+2601 (z=4.309): This quasar has a strong candidate damped absorber at z=3.96 with associated metal lines.
9. PSS J0131+0633 (z=4.417): This quasar has two very weak candidate damped absorbers at z=3.17 and 3.69. C IV is also detected at z=3.69.
10. PSS J0133+0400 (z=4.154): This spectrum has four candidate damped absorbers. The absorbers at z=3.69 and 3.77 have estimated column densities above the formal definition of DLA ($N_{\text{HI}} \geq 10^{20.3}$ atoms cm $^{-2}$) and the absorbers at z=3.08 and 4.00 are below that threshold. Associated metal lines are detected for all of the candidate DLAs.
11. PSS J0134+3307 (z=4.532): The quasar has a DLA at z=3.76 with associated metal lines.
12. PSS J0137+2837 (z=4.258): This quasar exhibits broad absorption lines. The spectrum is not used in our absorption line survey.
13. PSS J0152+0735 (z=4.051): This quasar has an excellent DLA candidate at z=3.84 with associated metal lines, which is also detected as a Lyman limit system.
14. PSS J0207+0940 (z=4.136): This quasar exhibits strong intrinsic absorption features. The spectrum is not used in our absorption line survey.
15. PSS J0209+0517 (z=4.174): This quasar has weak emission lines but exhibits two DLA candidates at z=3.66 and 3.86. Both have associated metal absorption features.
16. SDSS J0211–0009 (z=4.874): We detect one weak candidate DLA in this quasar at z=4.64. Si II is also detected at that redshift.
17. BR J0234–1806 (z=4.301): This quasar shows one weak absorption candidate at z=3.69 with associated metal lines.
18. PSS J0248+1802 (z=4.422): This spectrum shows no DLA candidates.
19. BR J0301–5537 (z=4.133): This quasar shows three DLA candidates at z=3.22, 3.38, and 3.71. All have associated metal lines but the two higher redshift candidates have estimated column densities below 2×10^{20} atoms cm $^{-2}$.
20. BR J0307–4945 (z=4.728): The spectrum shows the highest redshift damped absorber currently known at z=4.46 with an estimated column density of log $N_{\text{HI}} = 20.8$. Associated metal lines of Si II, O I, C II, Si IV, C IV, Fe II, and Al II are also detected at this redshift. The spectrum is shown in Figure 7. The spectrum of this object is discussed in more detail in McMahon et al., in preparation and Dessauges-Zavadsky et al. (2000). There is a weak DLA candidate at z=3.35 with no associated metal lines. This absorber is highly unlikely to be damped.
21. SDSS J0310–0014 (z=4.658): This quasar shows two candidate DLAs at z=3.42 and 4.34. The lower redshift system has an estimated column density above the DLA threshold. An associated Al II line is detected at z=3.424 but no metal lines associated with the higher redshift candidate are detected .
22. BR J0311–1722 (z=4.039): This quasar has a weak DLA candidate at z=3.73 which is also detected as a Lyman-limit system. Associated metal lines are also detected.

³<http://www.astro.caltech.edu/~george/z4.quasars>

23. PSS J0320+0208 ($z=3.840$): This quasar exhibits broad absorption lines. The spectrum is not used in our absorption line survey.
24. BR J0324–2918 ($z=4.622$): No DLA candidates are detected in this spectrum.
25. BR J0334–1612 ($z=4.363$): A DLA candidate at $z=3.56$ with associated Si II is detected in this quasar. This candidate has previously been detected (Storrie-Lombardi & Wolfe 2000) with a lower estimated column density ($\log N_{\text{HI}}=20.6$) than we measure .
26. SDSS J0338+0021 ($z=5.010$): This quasar has one DLA candidate at $z=4.06$ with associated metals detected.
27. BR J0355–3811 ($z=4.545$): No DLA candidates are detected in this spectrum. There is a Mg II absorber at $z=2.228$.
28. BR J0403–1703 ($z=4.227$): No DLA candidates are detected. No metal lines could be identified in this spectrum.
29. BR J0415–4357 ($z=4.070$): A weak DLA candidate with associated metal lines is detected at $z=3.81$.
30. BR J0419–5716 ($z=4.461$): Three weak DLA candidates are detected just above the Lyman-limit edge in this spectrum at $z=2.82$, 2.90, and 2.98. One associated metal line is detected from each of the two lower redshift systems.
31. BR J0426–2202 ($z=4.320$): A very high column density candidate ($\log N_{\text{HI}}=21.1$) is detected at $z=2.98$ with associated Al II.
32. PMN J0525–3343 ($z=4.383$): No DLA candidates are detected in this spectrum. Two Mg II absorbers are detected at $z=1.570$ and 2.006.
33. BR J0529–3526 ($z=4.413$): A weak DLA candidate with associated metal lines is detected at $z=3.57$.
34. BR J0529–3552 ($z=4.172$): A ‘doublet’ of weak DLA candidates is detected at $z=3.68$ and 3.70. No associated metals are detected at these redshifts.
35. BR J0714–6455 ($z=4.462$): No DLA candidates are detected in this spectrum.
36. PSS J0747+4434 ($z=4.430$): Two DLA candidates are detected at $z=3.76$ and 4.02. The higher redshift system also has associated metal lines.
37. RX J1028–0844 ($z=4.276$): Two weak DLA candidates with associated metals are detected at $z=3.42$ and 4.05.
38. PSS J1048+4407 ($z=4.381$): This quasar exhibits broad absorption lines. The spectrum is not used in our absorption line survey.
39. PSS J1057+4555 ($z=4.116$): Three DLA candidates are detected at $z=2.90$, 3.05, and 3.32. The candidate absorber at $z=3.32$ has been confirmed as damped in a higher resolution spectrum. It has a redshift of $z=3.3172$ and a column density $\log N_{\text{HI}}=20.34$ (Lu, Sargent & Barlow 1998). The estimated column density ($\log N_{\text{HI}}=20.3$) for the $z=3.05$ is identical to the estimate reported in Storrie-Lombardi & Wolfe (2000).
40. PSS J1159+1337 ($z=4.073$): This quasar has a DLA candidate at $z=3.72$ with several associated metal lines.
41. PSS J1253–0228 ($z=4.007$): This quasar has two candidate damped absorbers. One absorber at $z=2.78$ has a very high estimated column density ($\log N_{\text{HI}}=21.4$) and an associated Al II line is detected. This is the highest column density absorber in our survey. Another absorber at $z=3.60$ is highly unlikely to be damped, with an estimated column density of $\log N_{\text{HI}}=19.7$, but does have several associated metal lines.
42. BR J1310–1740 ($z=4.185$): This quasar has a weak damped candidate at $z=3.43$. Associated metal lines are also detected at this redshift.
43. BR J1330–2522 ($z=3.949$): This quasar has two weak DLA candidates at $z=2.91$ and 3.08. The higher redshift system has associated metal lines.
44. FIRST J1410+3409 ($z=4.351$): There is a weak candidate damped absorber at $z=3.43$ with no associated metal lines. In this spectrum the redshift path surveyed for damped absorbers is not continuous due to a large noise spike in the forest at $z \approx 3.59$.
45. PSS J1438+2538 ($z=4.234$): This quasar exhibits broad absorption lines. The spectrum is not used in our absorption line survey.
46. PSS J1456+2007 ($z=4.249$): There are two weak DLA candidates at $z=3.22$ and 4.16. The lower redshift system also has associated metal lines.
47. BR J1603+0721 ($z=4.385$): No DLA candidates are detected in this spectrum.
48. PSS J1618+4125 ($z=4.213$): There is a DLA candidate at $z=3.92$ with associated metal lines.
49. PSS J1633+1411 ($z=4.351$): There is a weak DLA candidate at $z=3.90$ with associated metal lines.
50. PSS J1646+5514 ($z=4.037$): No DLA candidates are detected in this spectrum.
51. PSS J1721+3256 ($z=4.031$): No DLA candidates are detected in this spectrum.
52. RX J1759+6638 ($z=4.320$): There is a DLA candidate at $z=3.40$ with associated metal lines.

53. PSS J1802+5616 ($z=4.158$): There are four damped absorber candidates detected in this spectrum at $z=3.39$, 3.56, 3.76, and 3.80. Only the absorber at $z=3.76$ has an estimated column density above the formal definition of DLA ($N_{HI} \geq 10^{20.3}$ atoms cm $^{-2}$). Associated metal lines are detected for the $z=3.39$ and 3.80 absorbers.
54. BR J2017–4019 ($z=4.131$): This quasar exhibits strong intrinsic absorption at the quasar emission redshift. The C IV and Si IV emission lines are completely absorbed. The spectrum is not used in our absorption line survey.
55. PSS J2122–0014 ($z=4.114$): This spectrum shows two DLA candidates at $z=3.20$ and 4.00. We estimate the column density of the lower redshift system to be $\log N_{HI}=20.3$, but this may be an overestimating as the Ly α line at $z=3.20$ is at the same position as the Ly β line at $z=4.00$. Associated metal lines are detected for both absorption systems.
56. BR J2131–4429 ($z=3.834$): This quasar exhibits broad absorption lines. The spectrum is not used in our absorption line survey.
57. PMN J2134–0419 ($z=4.334$): This quasar has one weak DLA candidate at $z=3.27$ with associated metal lines.
58. PSS J2154+0335 ($z=4.363$): This quasar has two DLA candidates at $z=3.61$ and 3.79. Metal lines are detected for both, but only the lower redshift system has an estimated column density above 2×10^{20} atoms cm $^{-2}$.
59. PSS J2155+1358 ($z=4.256$): This quasar has a very high column density ($\log N_{HI} = 21.1$) DLA candidate at $z=3.32$. Associated metal lines are also detected at this redshift.
60. BR J2216–6714 ($z=4.469$): This quasar has three weak DLA candidates at $z=3.27$, 4.28, and 4.32. At least one associated metal line has been detected for each.
61. PSS J2241+1352 ($z=4.441$): This quasar has two DLA candidates at $z=3.65$ and 4.28. The lower redshift system has an estimated column density below the formal definition of DLA ($N_{HI} \geq 10^{20.3}$ atoms cm $^{-2}$). Both have associated metal lines.
62. DMS B2247–0209 ($z=4.335$): This quasar exhibits broad absorption lines. The spectrum is not used in our absorption line survey.
63. PSS J2315+0921 ($z=4.412$): This quasar exhibits strong intrinsic absorption at the quasar emission redshift. The C IV and Si IV emission lines are almost completely absorbed. It is similar in character to the spectrum of BR J2017–4019. The spectrum is not used in our absorption line survey.
64. BR J2317–4345 ($z=3.943$): This quasar has a strong DLA candidate at $z=3.49$ with associated metal lines.
65. BR J2328–4513 ($z=4.359$): There is a weak DLA candidate at $z=3.04$. Si II is detected at this redshift but may be blended with C IV at $z=3.719$.
66. PSS J2344+0342 ($z=4.239$): There are two very high column density DLA candidates at $z=2.68$ and 3.21. Both have associated metal lines.
67. BR J2349–3712 ($z=4.208$): There is a weak DLA candidate at $z=3.69$ with associated Si II.

9. CONCLUSIONS

We have presented the spectra of sixty-six $z \gtrsim 4$ bright quasars with ~ 5 Å resolution (FWHM) and signal-to-noise ratio ranging from 10 to 30. Twenty-six new damped Ly α absorption candidates (column densities $N_{HI} \geq 2 \times 10^{20}$ atoms cm $^{-2}$) and forty-nine new Lyman-limit systems ($N_{HI} \geq 1.6 \times 10^{17}$ atoms cm $^{-2}$), fifteen of which are within 3000 km s $^{-1}$ of the quasar emission, have been discovered. The space density and column density evolution of these systems will be analyzed in subsequent papers. Higher resolution observations are needed in order to confirm the column density measurement and to differentiate the multiple systems among the DLA candidates presented here, and in order to make detailed analysis of the metallicity content of these absorbers. These high-column density systems can also be used to measure the neutral hydrogen content of the Universe over a large redshift range, thus probing the formation epoch of these objects and tracing the gas from which stars form. Analyzed in conjunction with previous studies, our new survey will provide enough data to help draw statistically more significant conclusions on these issues at high redshift.

The authors are indebted to the referee, Julia Kennefick, for helpful comments. CP warmly thanks Max Pettini for useful suggestions on an earlier version of this manuscript, Bob Carswell for help with his code and PPARC & the Isaac Newton Trust for support. LSL is grateful to the staff at CTIO for their expert assistance in obtaining some of the observations presented here. RGM would like to thank the Royal Society for support. This research has made use of the NASA/IPAC Extragalactic Database (NED) which is operated by the Jet Propulsion Laboratory, California Institute of Technology, under contract with the National Aeronautics and Space Administration. This paper is based on observations obtained at the William Herschel Telescope which is operated on the island of La Palma by the Isaac Newton Group in the Spanish Observatorio del Roque de los Muchachos of the Instituto de Astrofísica de Canarias, on observations made at the Cerro Tololo Intra-American Observatory which is operated by the Association of Universities for Research in Astronomy, under a cooperative agreement with the National Science Foundation as part of the National Optical Astronomy Observatories and on data obtained at the W.M. Keck Observatory, which is operated as a scientific partnership among the California Institute of Technology, the University of California and the National Aeronautics and Space Administration. The Observatory was made possible by the generous financial support of the W.M. Keck Foundation.

REFERENCES

- Abel, T., & Mo, H. 1998 ApJ, 494, L151
 Bergeson, S., & Lawler, J. 1993, ApJ, 414, L137
 Cardelli, J.A., Meyer, D.M., Jura, M., & Savage, B.D. 1995, ApJ, 452, 275
 Cole, S., Aragon-Salamanca, A., Frenk, C., Navarro, J., & Zepf, S. 1994, MNRAS, 271, 781
 Dessauges-Zavadsky, M., D'Odorico, S., McMahon, R.G., Molaro, P., Ledoux, C., Peroux C., & Storrie-Lombardi, L.J. 2000, A&A, submitted
 Fan, X. et al. 2000, AJ, 120, 1167
 Fan, X. et al. 1999, AJ, 118, 1
 Francis, P., Hewett, P., Foltz, C., Chaffee, F., Weymann, R., & Morris, S. 1991, ApJ, 373, 465
 Fynbo, J., Thomsen B., & Moller, P. 2000 A&A, 353, 457
 Gunn, & Peterson 1965, ApJ, 142, 1633
 Hall, P.B., Osmer, P.S., Green, R.F., Porter, A.C., & Warren, S.J. 1996, ApJ, 462, 614
 Henry, J.P., Gioia, I.M., Boehringer, H., Bower, R.G., Briel, U.G., Hasinger, G.H., Aragon-Salamanca, A., Castander, F.J., Ellis, R.S., Huchra, J.P., Burg, R., & McLean, B. 1994, AJ, 107, 4
 Hook, I.M. et al. in preparation
 Jimenez, R., Bowen, D.V. & Matteucci, F. 1999, ApJ, 514, L83
 Kauffmann, G., & Haehnelt, M. 2000, MNRAS, 311, 576
 Kauffmann, G., White, S., & Guiderdoni, B. 1993, MNRAS, 264, 201
 Kennefick, J., De Carvalho, R., Djorgovski, G., Wilber, M., Dickson, E., & Weir, N. 1995a, AJ, 110, 78
 Kennefick, J., Djorgovski, S., & De Carvalho, R. 1995b, AJ, 100, 2553
 Lanzetta, K.M., Wolfe, A.M., Turnshek, D.A., Lu, L., McMahon, R.G., & Hazard, C. 1991, ApJS, 77, 1
 Lanzetta, K.M., Wolfe, A.M. & Turnshek, D.A. 1995, ApJ, 440, 435
 Ledoux, C., Petitjean, P., Bergeron, J., Wampler, E., & Srianand, R. 1998, A&A, 337, L51
 Levshakov, S., Agafonova, I., & Kegel, W. 2000, A&A, 355, L1
 Lu, L., Sargent, W.L.W., & Barlow, T.A. 1998, AJ, 115, 55
 Matteucci, F., Molaro, P., & Vladilo, G. 1997, *à*, 321, 45
 McMahon, R.G. et al. in preparation
 Molaro, P., Bonifacio, P., Centurion, M., & Vladilo, G. 1999, A&A, 349, L13
 Morton, D. 1991, ApJS, 77, 119
 Nussbaumer, H., Pettini, M., & Storey, P. 1981, A&A, 102, 351
 Peroux, C. et al. in preparation
 Pettini, M., Smith, L., King, D., & Hunstead R. 1997, ApJ, 486, 665
 Prochaska, J.X., & Wolfe, A. 1998, ApJ, 507, 113
 Prochaska, J.X., & Wolfe, A. 2000, ApJ, 533, L5
 Rao, S.M. & Turnshek, D.A. 2000, ApJS, 130, 1
 Sargent, W.L.W., Steidel, C.C., & Boksenberg, A. 1989, ApJS, 79, 703
 Schneider, D. and the Quasar Absorption Line Key Project 1993, ApJS, 87, 45.
 Somerville, R., Primack, J., & Faber, S. 2000, in press (astro-ph/0006364)
 Songaila, A., Hu, E., Cowie, L., & McMahon, R.G. 1999, ApJ, 525, L5
 Stengler-Larrea, E.A., Boksenberg, A., Steidel, C.C., Sargent, W.L.W., Bahcall, J.N., Bergeron, J., Hartig, G.F., Januzzi, B.T., Kirhakos, S., Savage, B.D., Schneider, D.P., Turnshek, D.A., & Weymann, R.J. 1995, ApJ, 444, 64
 Steidel, C., Dickinson, M. & Persson, S. 1994, ApJ, 437, L75
 Stern, D., Djorgovski, S.G., Perley, R.A., de Carvalho, R.R., & Wall, J.V. 2000, AJ, 119, 4
 Storrie-Lombardi, L.J., McMahon, R.G., Irwin, M.J., & Hazard, C. 1994, ApJ, 427, L13
 Storrie-Lombardi, L.J., McMahon, R.G., Irwin, M.J., & Hazard, C. 1996a, ApJ, 468, 128
 Storrie-Lombardi, L.J., McMahon, R.G., & Irwin, M.J. 1996b, MNRAS, 283, L79
 Storrie-Lombardi, L.J., Irwin, M.J., & McMahon, R.G. 1996c, MNRAS, 282, 1330
 Storrie-Lombardi, L.J., Irwin, M.J., McMahon, R.G., Hook, I.M. 2001, MNRAS, in press
 Storrie-Lombardi, L.J. & Wolfe, A.M. 2000, ApJ, 543, 552
 Warren, S.J., Hewett, P.C. & Osmer, P.S. 1991, ApJS, 76, 23
 Wolfe, A., Turnshek, D., Smith, H., & Cohen, R. 1986, ApJS, 61, 249
 Zickgraf, F.-J., Voges, W., Krautter, J., Thiering, I., Appenzeller, I., Mujica, R., & Serrano, A. 1997, A&A, 323, L21

TABLE 1
JOURNAL OF OBSERVATIONS

Quasar Name	Telescope	Date Observed	Exp. Time B/R ^a (secs)	Wide Slit	Ref
PSS J0003+2730	WHT	1998 Sep 22	3600/3600	yes	1
BR J0006-6208	CTIO	1998 Oct 14	3600	yes	3
BR J0030-5129	CTIO	1998 Oct 15	3600	yes	3
PSS J0034+1639	WHT	1998 Sep 22	3600/3600	yes	1
SDSS J0035+0040	CTIO	1999 Oct 10	8100	yes	4
PSS J0052+2405	WHT	1998 Sep 23	3600/3600	yes	2
Q J0054-2742	CTIO	1999 Oct 12	2700	yes	5
PSS J0106+2601	WHT	1998 Sep 24	3600/3600	yes	1
PSS J0131+0633	CTIO	1999 Oct 12	3600	no	2
PSS J0133+0400	CTIO	1999 Oct 12	3600	no	2
PSS J0134+3307	WHT	1998 Sep 22	3600/3600	yes	1
PSS J0137+2837	WHT	1998 Sep 24	5200/3600	yes	1
PSS J0152+0735	WHT	1998 Sep 24	3600/3600	yes	1
PSS J0207+0940	CTIO	1999 Oct 12	3600	no	2
PSS J0209+0517	CTIO	1999 Oct 12	2400	no	2
SDSS J0211-0009	CTIO	1999 Oct 10	8100	no	4
BR J0234-1806	CTIO	1999 Oct 09	5400	yes	3
PSS J0248+1802	WHT	1998 Sep 22	3600/3600	yes	6
BR J0301-5537	CTIO	1998 Oct 16	3600	yes	3
BR J0307-4945	CTIO	1998 Oct 14	5400	yes	3
SDSS J0310-0014	CTIO	1999 Oct 9	9900	no	4
BR J0311-1722	CTIO	1999 Oct 11	3600	yes	3
PSS J0320+0208	CTIO	1999 Oct 12	3600	no	2
BR J0324-2918	CTIO	1999 Oct 11	3600	yes	3
BR J0334-1612	WHT	1998 Sep 23	2740/1650	no	3
SDSS J0338+0021	Keck	1999 Feb 17	3000/3600	no	4
BR J0355-3811	CTIO	1998 Oct 15	3600	yes	3
BR J0403-1703	WHT	1999 Sep 19	1800/1800	no	7
BR J0415-4357	CTIO	1998 Oct 16	5400	yes	3
BR J0419-5716	CTIO	1998 Oct 14	3600	yes	3
BR J0426-2202	CTIO	1999 Oct 11	3000	yes	3
PMN J0525-3343	CTIO	1998 Oct 15	3600	yes	3
BR J0529-3526	CTIO	1998 Oct 14	5400	yes	3
BR J0529-3552	CTIO	1998 Oct 15	3600	yes	3
BR J0714-6455	CTIO	1998 Oct 15	3600	yes	3
PSS J0747+4434	WHT	1998 Sep 22	1800/1800	no	1
RX J1028-0844	WHT	1999 Mar 19	2700/2700	yes	8
PSS J1048+4407	WHT	1999 Mar 19	2700/2700	yes	9
PSS J1057+4555	WHT	1999 Mar 19	1800/1800	yes	9
PSS J1159+1337	WHT	1999 Mar 18	2700/2700	yes	1
PSS J1253-0228	WHT	1999 Mar 18	2700/1800	yes	2
BR J1310-1740	WHT	1999 Mar 19	2700/2700	yes	3
BR J1330-2522	WHT	1999 Mar 19	2700/2700	yes	3
FIRST J1410+3409	WHT	1999 Sep 19	2700/2700	yes	1
PSS J1438+2538	WHT	1999 Mar 18	2700/2700	yes	9
PSS J1456+2007	WHT	1999 Mar 18	2700/2700	yes	1
BR J1603+0721	WHT	1999 Mar 19	2700/2700	yes	3
PSS J1618+4125	WHT	1999 Mar 19	2700/2700	yes	1
PSS J1633+1411	WHT	1999 Mar 19	1800/1800	yes	2
PSS J1646+5514	WHT	1998 Sep 23	3600/3600	yes	1
PSS J1721+3256	WHT	1998 Sep 24	1800/3600	yes	1
RX J1759+6638	WHT	99/98 Mar 19/Sep 23	6300/6300	yes	10

TABLE 1—*Continued*

Quasar Name	Telescope	Date Observed	Exp. Time B/R ^a (secs)	Wide Slit	Ref
PSS J1802+5616	WHT	1999 Sep 14	1800	no	2
BR J2017–4019	CTIO	1998 Oct 14	3600	no	3
PSS J2122–0014	WHT	1998 Sep 22	3600/3600	no	1
BR J2131–4429	CTIO	1998 Oct 16	1800	no	3
PMN J2134–0419	CTIO	1999 Oct 12	5400	yes	11
PSS J2154+0335	WHT	1999 Sep 14	1800	no	2
PSS J2155+1358	CTIO	1999 Oct 10	3600	yes	2
BR J2216–6714	CTIO	1999 Oct 09	3600	yes	3
PSS J2241+1352	CTIO	1999 Oct 11	3600	yes	2
DMS B2247–0209	WHT	1998 Sep 24	5400/3600	yes	12
PSS J2315+0921	CTIO	1999 Oct 11	3600	yes	2
BR J2317–4345	CTIO	1998 Oct 14	3600	yes	3
BR J2328–4513	CTIO	1998 Oct 15	3600	yes	3
PSS J2344+0342	CTIO	1999 Oct 11	3600	yes	2
BR J2349–3712	CTIO	1999 Oct 09	3600	yes	3

^aFor the quasars observed at the WHT the B/R designations give the exposure times through the blue and red arms of the ISIS spectrograph.

Note. — The quasar prefixes indication the following origin: BR = APM survey objects selected by B_J-R color excess; PSS = Second Palomar Sky Survey; PMN = Parkes-MIT-NRAO radio-selected objects; RX = X-ray selected; SDSS = Sloan Digital Sky Survey; and DMS = Deep Multicolor Survey

References. — (1) Stern et al. 2000; (2) G. Djorgovski's www page at <http://www.astro.caltech.edu/~george/z4.qsos>; (3) Storrie-Lombardi et al. 2000; (4) Fan et al. 1999; (5) Warren, Hewett, & Osmer 1991; (6) Kennefick et al. 1995a; (7) Storrie-Lombardi et al. 1996a; (8) Zickgraf et al. 1997; (9) Kennefick et al. 1995b; (10) Henry et al. 1994; (11) Hook et al. in preparation; (12) Hall et al. 1996

TABLE 2
QUASAR REDSHIFT MEASUREMENTS

Quasar	Ly α 1216Å	NV 1240Å	OI 1304Å	Si+O 1400Å	CIV 1549Å	Mean Redshift ^a	Note
PSS J0003+2730	4.255	4.205	4.261	4.248	4.233	4.240±0.022	
BR J0006–6208	4.505	...	4.471	...	4.388	4.455 ± 0.060	
BR J0030–5129	4.163	4.172	4.187	4.175	4.174	4.174 ± 0.009	
PSS J0034+1639	4.309	...	4.298	4.281	4.284	4.293 ± 0.013	
SDSS J0035+0040	4.737	...	4.758	...	4.746	4.747 ± 0.011	
PSS J0052+2405	1.90 ± 0.05	BAL, ^b
Q J0054–2742	4.464	4.464 ± 0.005	BAL
PSS J0106+2601	4.323	...	4.332	4.303	4.276	4.309 ± 0.025	
PSS J0131+0633	4.431	...	4.430	4.405	4.402	4.417 ± 0.015	
PSS J0133+0400	4.142	...	4.172	4.156	4.148	4.154 ± 0.013	
PSS J0134+3307	4.524	4.534	4.538	4.530	...	4.532 ± 0.006	
PSS J0137+2837	4.297	4.220	4.258 ± 0.054	BAL
PSS J0152+0735	4.042	...	4.064	4.047	4.049	4.051 ± 0.010	
PSS J0207+0940	4.132	4.142	4.134	4.136 ± 0.005	BAL
PSS J0209+0517	4.174	4.174 ± 0.007	
SDSS J0211–0009	4.874	4.874 ± 0.036	
BR J0234–1806	4.296	4.307	4.301 ± 0.008	
PSS J0248+1802	4.403	...	4.440	4.428	4.418	4.422 ± 0.016	
BR J0301–5537	4.146	4.125	4.129	4.133 ± 0.011	
BR J0307–4945	4.738	4.717	4.728 ± 0.015	
SDSS J0310–0014	4.645	4.701	...	4.645	4.639	4.658 ± 0.029	
BR J0311–1722	4.049	4.083	4.025	4.000	...	4.039 ± 0.036	
PSS J0320+0208	3.850	3.837	3.833	3.840 ± 0.009	BAL
BR J0324–2918	4.609	4.627	4.630	4.615	4.629	4.622 ± 0.009	
BR J0334–1612	4.356	...	4.383	4.364	4.350	4.363 ± 0.014	
SDSS J0338+0021	5.010	5.010 ± 0.033	
BR J0355–3811	4.530	...	4.567	4.549	4.533	4.545 ± 0.017	
BR J0403–1703	4.220	4.231	4.232	...	4.227	4.227 ± 0.005	
BR J0415–4357	4.064	...	4.075	4.069	4.072	4.070 ± 0.005	
BR J0419–5716	4.473	...	4.472	4.453	4.445	4.461 ± 0.014	
BR J0426–2202	4.322	4.324	...	4.319	4.314	4.320 ± 0.005	
PMN J0525–3343	4.417	4.384	4.349	4.383 ± 0.034	
BR J0529–3526	4.411	...	4.419	4.414	4.407	4.413 ± 0.005	
BR J0529–3552	4.172	...	4.181	4.167	4.167	4.172 ± 0.006	
BR J0714–6455	4.483	...	4.486	4.456	4.422	4.462 ± 0.030	
PSS J0747+4434	4.424	4.434	4.442	4.423	4.427	4.430 ± 0.008	
RX J1028–0844	4.235	4.317	4.276 ± 0.058	
PSS J1048+4407	4.422	4.367	4.354	4.381 ± 0.036	BAL
PSS J1057+4555	4.125	4.114	4.109	4.116 ± 0.008	
PSS J1159+1337	4.073	4.073 ± 0.014	
PSS J1253–0228	4.007	4.027	3.988	4.007 ± 0.019	
BR J1310–1740	4.201	4.179	4.175	4.185 ± 0.014	
BR J1330–2522	3.950	3.935	3.961	3.946	3.951	3.949 ± 0.009	
FIRST J1410+3409	4.357	4.351	4.370	4.338	4.338	4.351 ± 0.014	
PSS J1438+2538	4.275	4.193	4.232	4.234 ± 0.041	BAL
PSS J1456+2007	4.251	4.255	4.251	4.247	4.242	4.249 ± 0.005	
BR J1603+0721	4.393	...	4.404	...	4.359	4.385 ± 0.024	
PSS J1618+4125	4.212	...	4.220	4.215	4.206	4.213 ± 0.006	
PSS J1633+1411	4.354	4.347	4.352	4.351 ± 0.004	
PSS J1646+5514	4.071	...	4.058	4.018	4.003	4.037 ± 0.032	
PSS J1721+3256	4.034	...	4.046	4.028	4.016	4.031 ± 0.012	
RX J1759+6638	4.321	4.321	...	4.318	4.318	4.320 ± 0.002	

TABLE 2—*Continued*

Quasar	Ly α 1216Å	NV 1240Å	OI 1304Å	Si+O 1400Å	CIV 1549Å	Mean Redshift ^a	Note
PSS J1802+5616	4.171	4.146	...	4.158 ±.018	
BR J2017–4019	4.131	4.131 ±.013	BAL
PSS J2122–0014	4.156	4.105	4.080	4.114 ±.039	
BR J2131–4429	3.871	3.816	3.814	3.834 ±.032	BAL
PMN J2134–0419	4.330	4.344	...	4.331	4.330	4.334 ±.007	
PSS J2154+0335	4.360	...	4.367	4.363 ±.005	
PSS J2155+1358	4.285	4.269	4.216	4.256 ±.036	
BR J2216–6714	4.494	4.467	4.444	4.469 ±.025	
PSS J2241+1352	4.419	...	4.469	4.458	4.416	4.441 ±.027	
DMS B2247–0209	4.378	4.342	4.284	4.335 ±.048	BAL
PSS J2315+0921	4.412	4.412 ±.041	BAL
BR J2317–4345	3.949	3.931	3.950	3.943 ±.010	
BR J2328–4513	4.366	4.361	4.349	4.359 ±.009	
PSS J2344+0342	4.239	4.239 ±.052	
BR J2349–3712	4.221	4.169	4.231	...	4.211	4.208 ±.028	
median rest-frame composite spectrum	0.002		0.003	-0.001	-0.002	0.001	

^aThe error estimate is $\frac{\sigma}{\sqrt{n}}$.

^bThis object was originally in the PSS web page as a high redshift object. It has since been removed from that list. Our spectrum shows that it is a broad absorption line quasar at z=1.9.

Note. — BAL: These quasars exhibit broad absorption line characteristics.

TABLE 3
QUASAR MAGNITUDE MEASUREMENTS

Quasars	R ^a APM	R ^b	Filter ^c	Notes
PSS J0003+2730	18.3	17.8	e	
BR J0006-6208	18.3	19.2	R59	
BR J0030-5129	18.6	18.6	R59	
PSS J0034+1639	18.0	17.8	e	
SDSS J0035+0040	...	21.3	e	
PSS J0052+2405	17.4	17.4	e	BAL
Q J0054-2742	19.8	19.8	R59	BAL
PSS J0106+2601	18.5	18.3	e	
PSS J0131+0633	...	19.1	e	NC
PSS J0133+0400	18.3	18.0	e	NC
PSS J0134+3307	19.9	18.9	e	
PSS J0137+2837	18.3	18.6	e	BAL
PSS J0152+0735	18.7	18.0	e	
PSS J0207+0940	18.7	19.2	e	BAL, NC
PSS J0209+0517	17.8	17.8	e	NC
SDSS J0211-0009	...	21.5	e	NC
BR J0234-1806	18.8	19.2	R59	
PSS J0248+1802	17.7	17.6	e	
BR J0301-5537	19.0	18.9	R59	
BR J0307-4945	18.8	18.8	R59	
SDSS J0310-0014	20.7	21.0	R59	NC
BR J0311-1722	17.7	18.0	R59	
PSS J0320+0208	18.5	18.5	e	BAL, NC
BR J0324-2918	18.7	18.6	R59	
BR J0334-1612	17.9	19.2	R59	NC
SDSS J0338+0021	...	21.5	R63	NC
BR J0355-3811	17.9	18.2	R59	
BR J0403-1703	18.7	19.3	R63	NC
BR J0415-4357	18.8	18.9	R59	
BR J0419-5716	17.8	18.7	R59	
BR J0426-2202	17.9	18.0	R59	
PMN J0525-3343	18.4	18.7	R59	
BR J0529-3526	18.9	19.0	R59	
BR J0529-3552	18.3	18.5	R59	
BR J0714-6455	18.3	18.2	R59	
PSS J0747+4434	18.4	19.2	e	NC
RX J1028-0844	18.8	19.1	R59	
PSS J1048+4407	19.6	20.1	e	BAL
PSS J1057+4555	16.5	17.0	e	
PSS J1159+1337	17.1	17.1	e	
PSS J1253-0228	18.8	18.7	R59	
BR J1310-1740	19.5	19.2	R59	
BR J1330-2522	18.5	18.8	R59	
FIRST J1410+3409	19.9	20.7	e	
PSS J1438+2538	19.3	18.6	e	BAL
PSS J1456+2007	18.2	18.7	e	
BR J1603+0721	19.3	19.4	e	
PSS J1618+4125	18.5	19.0	e	
PSS J1633+1411	18.7	18.2	e	
PSS J1646+5514	17.1	16.5	e	
PSS J1721+3256	18.8	18.1	e	
RX J1759+6638	19.1	19.8	e	

TABLE 3—*Continued*

Quasars	R ^a APM	R ^b	Filter ^c	Notes
PSS J1802+5616	18.3	19.2	e	NC
BR J2017–4019	18.6	18.2	R59	BAL, NC
PSS J2122–0014	20.3	19.0	R59	NC
BR J2131–4429	18.3	18.4	R59	BAL, NC
PMN J2134–0419	20.0	19.2	R59	
PSS J2154+0335	19.0	18.6	e	NC
PSS J2155+1358	18.0	17.9	e	
BR J2216–6714	18.6	18.6	R59	
PSS J2241+1352	19.1	19.3	e	
DMS B2247–0209	19.8	19.0	R63	BAL
PSS J2315+0921	19.2	19.5	e	BAL
BR J2317–4345	19.0	18.5	R59	
BR J2328–4513	19.2	19.1	R59	
PSS J2344+0342	18.2	18.6	e	
BR J2349–3712	18.7	18.7	R59	

^aThe R magnitude from the photographic plates as measured by the APM. If no magnitudes are specified in this column, the quasar is not detected on the APM plates. The uncertainties in these magnitudes are estimated to be ± 0.25 .

^bThe R magnitude measured from the spectra as described in the text. The uncertainties in these magnitudes are estimated to be ± 0.1 .

^cR59 and R63 are UKST filters while e is the POSS1 filter.

Note. — The NC in the notes column means that the spectrum has not been corrected for slit losses. The BAL designation means the quasar exhibits broad absorption lines.

TABLE 4
SURVEY FOR LYMAN-LIMIT SYSTEMS

Quasar	z_{em}	z_{min}^a	z_{max}^b	z_{lls}	τ
PSS J0003+2730	4.240	2.858	4.198	3.97	2.6
BR J0006–6208	4.455	3.079	4.400	4.14	1.8
BR J0030–5129	4.174	3.079	4.122	3.37	1.0
PSS J0034+1639	4.293	2.858	4.240	4.26	4.1
SDSS J0035+0040 ^c	4.747	3.079	4.690	4.59	0.9
PSS J0106+2601 ^d	4.309	2.858	4.256	4.05	2.3
				3.96	2.7
PSS J0131+0633	4.417	3.079	4.363	4.37	2.1
PSS J0133+0400 ^d	4.154	3.079	4.102	4.02	1.5
				4.14	2.3
PSS J0134+3307	4.532	2.858	4.477	4.32	2.1
PSS J0152+0735 ^d	4.051	2.858	4.000	3.97	2.5
				3.88	2.8
PSS J0209+0517	4.174	3.079	4.122	3.97	2.6
SDSS J0211–0009	4.874	3.079	4.815	4.81	1.2
BR J0234–1806	4.301	3.079	4.248	4.27	2.4
PSS J0248+1802	4.422	2.858	4.368	4.13	2.0
BR J0301–5537	4.133	3.079	4.082	4.10	2.5
BR J0307–4945	4.728	3.079	4.671	4.50	2.8
SDSS J0310–0014 ^e	4.658	4.090	4.601
BR J0311–1722	4.039	3.079	3.989	3.76	2.0
BR J0324–2918	4.622	3.079	4.566	4.21	1.5
BR J0334–1612	4.363	2.858	4.309	4.24	1.4
SDSS J0338+0021	5.010	3.035	4.950	4.93	2.2
BR J0355–3811 ^d	4.545	3.079	4.490	4.39	1.6
				4.43	2.0
BR J0403–1703 ^f	4.227	4.175	4.175
BR J0415–4357	4.070	3.079	4.019	4.07	2.6
BR J0419–5716 ^d	4.461	3.079	4.406	4.14	1.3
				4.33	1.1
BR J0426–2202 ^c	4.320	3.079	4.267	3.97	0.8
PMN J0525–3343	4.383	3.079	4.329	4.09	2.3
BR J0529–3526	4.413	3.079	4.359	4.39	1.7
BR J0529–3552	4.172	3.079	4.120	4.10	2.8
BR J0714–6455	4.462	3.078	4.407	4.46	2.4
PSS J0747+4434	4.430	2.858	4.376	4.29	1.8
RX J1028–0844	4.276	2.857	4.223	3.62	3.0
PSS J1057+4555	4.116	2.857	4.065	3.90	4.4
PSS J1159+1337	4.073	2.857	4.022	3.77	4.0
PSS J1253–0228	4.007	2.857	3.957	3.65	3.5
BR J1310–1740	4.185	2.857	4.133	3.62	2.7
BR J1330–2522 ^d	3.949	2.857	3.900	3.72	1.8
				3.82	2.0
FIRST J1410+3409	4.351	2.857	4.297	3.87	1.2
PSS J1456+2007	4.249	2.857	4.197	4.17	3.5
BR J1603+0721	4.385	2.857	4.331	4.38	2.5
PSS J1618+4125	4.213	2.857	4.161	3.94	2.0
PSS J1633+1411 ^d	4.351	2.857	4.297	4.23	1.2
				4.33	1.4
PSS J1646+5514	4.037	2.858	3.987	4.03	5.3
PSS J1721+3256	4.031	2.858	3.981	4.03	2.5
RX J1759+6638 ^c	4.320	2.856	4.267	4.20	0.9
PSS J1802+5616 ^e	4.158	3.990	4.106

TABLE 4—*Continued*

Quasar	z_{em}	z_{min}^a	z_{max}^b	z_{lls}	τ
PSS J2122–0014	4.114	2.858	4.063	4.01	3.5
PMN J2134–0419	4.334	3.079	4.281	4.19	1.6
PSS J2154+0335 ^e	4.363	3.990	4.309
PSS J2155+1358	4.256	3.079	4.203	4.23	2.9
BR J2216–6714	4.469	3.079	4.414	3.98	1.2
PSS J2241+1352	4.441	3.079	4.387	4.31	1.8
BR J2317–4345	3.943	3.079	3.894	3.93	1.4
BR J2328–4513	4.359	3.079	4.305	4.19	2.0
PSS J2344+0342	4.239	3.079	4.187	3.98	1.5
BR J2349–3712	4.208	3.079	4.156	4.17	2.5

^a z_{min} corresponds to the smallest wavelength in the quasar spectrum.

^b z_{max} is 3000 km s⁻¹ blueward of the quasar emission redshift.

^cSystems with optical depth, τ , < 1 are excluded from the total count of LLS because they do not conform to the formal definition of Lyman-limit Systems.

^dIn case where two breaks were detected, only the highest system is taken into account in the final count for LLS.

^eNo LLS have been detected over the specified redshift range.

^fThe signal-to-noise ratio of this spectrum is too low to enable LLS detection.

TABLE 5
SURVEY FOR DAMPED LYMAN- α ABSORPTION SYSTEMS

Quasar	z_{em}	z_{min}	z_{max}	z_{abs}	W (Å)	$\log N_{\text{HI}}$ (cm $^{-2}$)	Metal Lines	z_{metal}	Note
PSS J0003+2730	4.240	2.718	4.188	3.51	7.6	20.0	Si II 1527 Fe II 1608 Al II 1671 C II 1334 Si IV 1400 C IV 1549 Al II 1671	3.513 3.510 3.512 3.893 3.893 3.893 3.891	
				3.89	9.0	20.2			
BR J0006–6208	4.455	2.944	4.400	2.97	15.6	20.7	Si II 1808 Al II 1671 Si II 1527 Fe II 1608 C II 1334	2.965 3.193 3.776 3.780 4.150	a b
				3.20	21.6	20.9			
				3.78	22.5	21.0			
BR J0030–5129	4.174	2.304	4.122	4.14	7.9	20.1	Fe II 2261 Fe II 2344 Fe II 2383	2.449 2.452 2.451	
PSS J0034+1639	4.293	2.981	4.240	3.75	8.9	20.2	Si II 1527 C IV 1549 Si II 1260 O I 1302 C II 1334 Si IV 1400 Si II 1527 C IV 1549 Fe II 1608	3.752 3.754 4.252 4.262 4.282 4.281 4.282 4.281 4.281	
				4.26	24.9	21.1			
SDSS J0035+0040	4.747	3.309	4.690	
PSS J0106+2601	4.309	2.764	4.256	3.96	13.5	20.5	Ly β C II 1334 Si IV 1400 C IV 1549	3.96 3.958 3.957 3.959	b
PSS J0131+0633	4.417	3.014	4.363	3.17	6.6	19.9	
				3.61	5.5	19.8	C IV 1549	3.609	
PSS J0133+0400	4.154	2.865	4.102	3.08	8.2	20.1	C IV 1549 Si II 1808 Si II 1527 Al II 1671 C II 1334 Si IV 1400 Si II 1527 Fe II 1608 Al II 1671 Si II 1260 O I 1302 Si IV 1400 Si II 1527	3.083 3.085 3.691 3.690 3.771 3.771 3.771 3.770 3.771 3.993 3.994 3.996 3.993	
				3.69	11.9	20.4			
				3.77	12.5	20.5			
				4.00	8.6	20.1			
PSS J0134+3307	4.532	2.562	4.477	3.76	14.8	20.6	Si II 1527 C IV 1549 Al II 1671	3.761 3.775 3.780	d
PSS J0152+0735	4.051	1.890	4.000	3.84	17.0	20.7	Ly β O I 1302 C II 1334	3.84 3.841 3.842	b
PSS J0209+0517	4.174	2.759	4.122	3.66	10.1	20.3	Al II 1671	3.664	
				3.86	15.2	20.6	Ly β	3.86	

TABLE 5—*Continued*

Quasar	z_{em}	z_{min}	z_{max}	z_{abs}	W (Å)	$\log N_{\text{HI}}$ (cm $^{-2}$)	Metal Lines	z_{metal}	Note
							Si II 1304	3.862	
							C II 1334	3.862	
SDSS J0211–0009	4.874	3.402	4.815	4.64	7.5	20.0	Si II 1527	4.645	
BR J0234–1806	4.301	2.971	4.248	3.69	8.7	20.2	Si IV 1400	3.694	
							Al II 1671	3.692	
PSS J0248+1802	4.422	2.810	4.368	
BR J0301–5537	4.133	2.825	4.082	3.22	10.4	20.3	Si II 1527	3.220	
				3.38	7.9	20.1	Si II 1527	3.377	
				3.71	7.0	20.0	C II 1334	3.705	
							C IV 1549	3.701	
BR J0307–4945	4.728	3.138	4.671	3.35	6.0	19.8	
				4.46	18.6	20.8	Ly β	4.46	b
							O I 1302	4.465	
							Si II 1304	4.466	
							C II 1334	4.465	
							Si IV 1400	4.464	
							Si II 1527	4.466	
							C IV 1549	4.464	
							Fe II 1608	4.466	
							Al II 1671	4.466	
SDSS J0310–0014	4.658	3.087	4.601	3.42	13.2	20.5	Al II 1671	3.424	
				4.34	8.6	20.1	
BR J0311–1722	4.039	2.591	3.989	3.73	8.7	20.2	O I 1302	3.733	
							Si II 1304	3.733	
							C II 1334	3.733	
BR J0324–2918	4.622	2.900	4.566	
BR J0334–1612	4.363	3.080	4.309	3.56	24.5	21.0	Si II 1527	3.558	
SDSS J0338+0021	5.010	3.528	4.950	4.06	11.8	20.4	Si II 1527	4.059	
							Al II 1671	4.066	
BR J0355–3811	4.545	3.030	4.490	
BR J0403–1703	4.227	2.992	4.175	
BR J0415–4357	4.070	2.813	4.019	3.81	7.1	20.1	Ly β	3.81	
							O I 1302	3.806	
							Si II 1304	3.806	
							C II 1334	3.806	
							Si II 1527	3.806	
BR J0419–5716	4.461	2.820	4.406	2.82	7.4	20.0	Fe II 2344	2.819	
				2.90	8.8	20.2	Fe II 2344	2.896	
				2.98	5.1	19.7	
BR J0426–2202	4.320	2.544	4.267	2.98	26.2	21.1	Al II 1671	2.982	
PMN J0525–3343	4.383	2.829	4.329	
BR J0529–3526	4.413	3.023	4.359	3.57	8.5	20.1	Fe II 1608	3.573	
							Al II 1671	3.571	
BR J0529–3552	4.172	2.821	4.120	3.68	7.6	20.0	
				3.70	7.6	20.0	
BR J0714–6455	4.462	3.050	4.407	
PSS J0747+4434	4.430	2.764	4.376	3.76	10.3	20.3	
				4.02	15.4	20.6	Ly β	4.02	
							C II 1334	4.020	
							Al II 1671	4.017	
RX J1028–0844	4.276	2.533	4.223	3.42	8.0	20.1	Ly β	3.422	
							Si II 1527	3.423	

TABLE 5—*Continued*

Quasar	z_{em}	z_{min}	z_{max}	z_{abs}	W (Å)	$\log N_{\text{HI}}$ (cm $^{-2}$)	Metal Lines	z_{metal}	Note
PSS J1057+4555	4.116	2.652	4.065	4.05	5.0	19.7	Al II 1671	3.422	
				2.90	8.0	20.1	Al II 1671	4.047	e
				3.05	10.0	20.3	Al II 1671	2.910	
							Fe II 1608	3.061	
							Al II 1671	3.051	
							Si II 1808	3.049	
							Si II 1527	3.316	
							Al II 1671	3.317	
							Ly β	3.72	b,f
							C II 1334	3.723	
PSS J1159+1337	4.073	2.563	4.022	3.32	8.9	20.2	Si IV 1400	3.723	
				3.72	10.3	20.3	Si II 1527	3.723	
							C II 1334	3.723	
							Si IV 1400	3.723	
							Si II 1527	3.723	
PSS J1253–0228	4.007	2.498	3.957	2.78	38.5	21.4	C IV 1549	3.724	
				3.60	5.2	19.7	Al II 1671	3.723	
							Al II 1671	3.723	
							Si IV 1400	3.603	
							C IV 1549	3.602	
BR J1310–1740	4.185	2.508	4.133	3.43	8.1	20.1	Fe II 1608	3.599	
							Si II 1527	3.435	
							C IV 1549	3.434	
							Al II 1671	3.433	
BR J1330–2522	3.949	2.578	3.900	2.91	7.5	20.0	
				3.08	5.7	19.8	Si II 1527	3.082	
							C IV 1549	3.081	
							Fe II 1608	3.080	
							Al II 1671	3.080	
FIRST J1410+3409	4.351	3.026	3.578	3.43	8.2	20.1	
				3.602	4.297	
PSS J1456+2007	4.249	2.878	4.197	3.22	5.6	19.8	Si II 1527	3.223	
							Si II 1808	3.221	
BR J1603+0721	4.385	3.062	4.331	...	6.8	19.9	
							
PSS J1618+4125	4.213	2.820	4.161	3.92	12.9	20.5	Si IV 1400	3.920	
							Si II 1527	3.914	
PSS J1633+1411	4.351	2.536	4.297	3.90	5.8	19.8	C IV 1549	3.895	
							Fe II 1608	3.906	
PSS J1646+5514	4.037	2.772	3.987	
PSS J1721+3256	4.031	2.791	3.981	
RX J1759+6638	4.320	2.804	4.267	3.40	12.4	20.4	Si II 1527	3.398	
							C IV 1549	3.397	
							Al II 1671	3.397	
							Si II 1527	3.386	
							C IV 1549	3.389	
PSS J1802+5616	4.158	2.891	4.106	3.39	8.3	20.1	
							
							
							
							
PSS J2122–0014	4.114	2.350	4.063	3.20	10.7	20.3	Si II 1527	3.206	
							C IV 1549	3.206	
							Fe II 1608	3.205	
							Al II 1671	3.206	
							Si II 1260	3.999	b

TABLE 5—Continued

Quasar	z_{em}	z_{min}	z_{max}	z_{abs}	W (Å)	$\log N_{\text{HI}}$ (cm $^{-2}$)	Metal Lines	z_{metal}	Note
PMN J2134–0419	4.334	2.903	4.281	3.27	7.0	20.0	Si II 1527 C IV 1549 C IV 1549 Fe II 1608	4.001 4.000 3.262 3.269	
PSS J2154+0335	4.363	2.979	4.309	3.61	11.3	20.4	Si II 1527 3.79 C IV 1549	3.623 3.778	
PSS J2155+1358	4.256	2.940	4.203	3.32	24.6	21.1	Si II 1527 C IV 1549 Fe II 1608 Al II 1671	3.316 3.313 3.316 3.314	h
BR J2216–6714	4.469	2.795	4.414	3.37	7.0	20.0	C IV 1549 Si II 1808 4.28 Ly β O I 1302	3.369 3.364 4.28 4.28 4.262	
PSS J2241+1352	4.441	3.027	4.387	3.65	7.2	20.0	Si II 1304 Si II 1808 4.28 O I 1302 Si II 1304 C II 1334 Si IV 1400 Si II 1527 Fe II 1608	4.323 3.647 4.28 4.282 4.284 4.282 4.286 4.283 4.284	
BR J2317–4345	3.943	2.448	3.894	3.49	20.2	20.9	Si IV 1400 C IV 1549 Fe II 1608	3.483 3.486 3.491	
BR J2328–4513	4.359	2.926	4.305	3.04	8.3	20.1	Si II 1808	3.041	i
PSS J2344+0342	4.239	2.696	4.187	2.68	23.0	21.0	Si II 1808 Fe II 2260 Fe II 2367 3.21 21.1 20.9	2.678 2.684 2.678 C IV 1549 Fe II 1608 Al II 1671 Si II 1808	j
BR J2349–3712	4.208	2.847	4.156	3.69	9.5	20.2	Si II 1527	3.691	

^aFe II 1608 at $z=3.780$ is at the same position as Fe II 2600 at $z=1.958$.

^bAlso detected as a Lyman-limit system.

^cThis damped system is within 3000 km s $^{-1}$ of the quasar emission redshift but we have included it in this table due to the fact that it is the first damped absorber detected at a redshift $z > 4$ with a column density $\log N_{\text{HI}} > 21$.

^dSi II 1527 at $z=3.761$ is at the same position as C IV 1549 at $z=3.686$.

^eAl II 1671 at $z=4.047$ is at the same position as Mg I 2853 at $z=1.956$.

^fThis damped absorption line has a very narrow core but strong damping wings are visible on both sides of the line.

^gThe Ly α line may be blended with Ly β at $z=4.00$, therefore the column density may be overestimated. This quasar has an unusually rich absorption spectrum, with many C IV absorbers redward of the Ly α emission.

^hSi II 1527 at $z=3.316$ is at the same position as Fe II 2260 at $z=1.915$.

ⁱSi II 1808 at $z=3.041$ is blended with C IV 1549 at $z=3.719$.

^jThis damped absorption candidate is just below the minimum redshift determined with our detection algorithm. It is likely to be real but requires confirmation with a higher signal-to-noise spectrum.

TABLE 6
METAL LINES REST WAVELENGTHS

Ion	λ (Å)	Ref.
N V	1238.821	1
N V	1242.804	1
Si II	1260.4221	1
Si II	1304.3702	1
C II	1334.5323	1
Si IV	1393.7550	1
Si IV	1402.7700	1
Si II	1526.7066	1
C IV	1548.1950	1
C IV	1550.7700	1
Fe II	1608.4511	1
Fe II	1611.2005	1
Al II	1670.7874	1
Si II	1808.0126	2
Fe II	2260.7805	1
Fe II	2344.2140	1
Fe II	2367.5910	3
Fe II	2374.4612	4
Fe II	2382.7650	4
Fe II	2586.6500	4
Fe II	2600.1729	4
Mg II	2796.3520	1
Mg II	2803.5310	1
Mg I	2852.9641	1

References. — (1)
Morton 1991; (2) Bergeson
& Lawler 1993; (3) Nuss-
baumer, Pettini & Storey
1982; (4) Cardelli & Savage
1995

TABLE 7
IDENTIFICATION OF METAL ABSORPTION LINES

Quasar	z_{em}	λ_{obs} (Å)	W_{obs} (Å)	Ion	λ_{rest} (Å)	z
PSS J0003+2730	4.240	6530.3	5.6	C II	1334	3.893
		6819.2	2.1	Si IV	1393	3.893
		6863.6	1.6	Si IV	1402	3.893
		6889.8	1.4	Si II	1527	3.513
		7254.7	1.7	Fe II	1608	3.510
		7320.6	1.3	C IV	1548	3.729
		7332.6	0.8	C IV	1551	3.728
		7468.7	3.3	Si II	1527	3.892
		7538.6	2.3	Al II	1671	3.512
		7574.3	3.9	C IV	1548	3.892
		7589.6	2.7	C IV	1551	3.894
		8042.5	0.9	C IV	1548	4.195
		8054.2	0.5	C IV	1551	4.194
		8078.6	0.4
		8172.2	3.6	Al II	1671	3.891
		8293.3	2.4	Mg II	2796	1.966
		8314.8	1.4	Mg II	2803	1.966
BR J0006-6208	4.455	6744.9	0.9	Al II	1608	3.193
		6872.2	0.6	C II	1334	4.150
		6903.8	0.9
		6933.6	2.4	Fe II	2344	1.958
		7022.1	2.5	Fe II	2374	1.957
		7033.3	2.0
		7048.1	4.7	Fe II	2383	1.958
		7105.9	1.6
		7168.6	1.3	Si II	1808	2.965
		7252.8	2.0
		7292.0	1.2	Si II	1527	3.776
		7428.1	0.7
		7650.6	2.6	Fe II	2586	1.958
		7689.2	4.3	Fe II	2600	1.957
		...	or	Fe II	1608	3.781
		8271.8	6.1	Mg II	2796	1.958
		8292.6	5.4	Mg II	2803	1.958
		8396.7	1.1
		8438.4	1.4	Mg I	2853	1.958
BR J0030-5129	4.174	6743.6	2.3
		6869.0	2.6	C IV	1548	3.437
		6880.3	1.4	C IV	1551	3.437
		7165.8	1.3
		7224.4	1.2
		7658.7	1.7	C IV	1548	3.947
		7670.6	1.6	C IV	1551	3.946
		7798.2	1.2	Fe II	2261	2.449
		8091.6	2.7	Fe II	2344	2.452
		8223.0	1.8	Fe II	2383	2.451
		8355.1	5.0
		8384.6	3.7
		8987.4	2.9
		9002.7	3.8
		6521.3	4.8	N V	1240	4.259
PSS J0034+1639	4.293	6560.3	2.6	Fe II	2344	1.798

TABLE 7—Continued

Quasar	z_{em}	λ_{obs} (Å)	W_{obs} (Å)	Ion	λ_{rest} (Å)	z
		6620.2	1.5	Si II	1260	4.252
		6645.1	1.4	Fe II	2374	1.799
		6657.1	3.0	C IV	1548	3.300
		6668.3	3.2	Fe II	2383	1.799
		...	or	C IV	1551	3.300
		6817.1	4.7
		6836.6	0.9
		6851.8	0.5	O I	1302	4.262
		6878.7	3.4	C IV	1548	3.443
		6890.6	2.2	C IV	1551	3.443
		6932.8	1.9	C IV	1548	3.478
		6945.6	1.3	C IV	1551	3.479
		7007.8	1.1
		7049.2	3.9	C II	1334	4.282
		7238.6	3.4
		7255.0	1.3	Si II	1527	3.752
		7279.9	4.8	Fe II	2600	1.800
		7318.9	0.6
		7330.5	1.1
		7361.5	2.2	Si IV	1393	4.281
		...	or	C IV	1549	3.752
		7407.0	0.9	Si IV	1402	4.281
		7825.9	4.9	Mg II	2796	1.799
		7845.8	4.2	Mg II	2803	1.799
		7983.2	0.6	Mg I	2853	1.798
		8063.7	2.3	Si II	1527	4.282
		8089.6	4.2	C IV	1548	4.225
		8103.4	2.1	C IV	1551	4.225
		8131.5	1.4
		8176.1	1.2	C IV	1548	4.281
		8190.5	0.8	C IV	1551	4.282
		8495.0	1.5	Fe II	1608	4.281
SDSS J0035+0040	4.747	7132.3	2.4	N V	1240	4.752
		8736.1	2.5
		9002.2	5.1
PSS J0106+2601	4.309	6617.0	1.3	C II	1334	3.958
		6798.8	2.4
		6846.3	1.3
		6864.5	1.3
		6909.3	2.0	Si IV	1393	3.957
		6955.5	1.3	Si IV	1402	3.958
		7465.1	1.5	C IV	1548	3.822
		7477.5	0.7	C IV	1551	3.822
		7494.4	2.2
		7677.9	3.2	C IV	1548	3.959
		7690.2	2.0	C IV	1551	3.959
		8014.1	1.5
		8230.3	2.2
		8249.1	1.3
		8268.2	1.9
PSS J0131+0633	4.417	6770.6	1.0
		6792.0	1.3

TABLE 7—Continued

Quasar	z_{em}	λ_{obs} (Å)	W_{obs} (Å)	Ion	λ_{rest} (Å)	z
		7135.7	1.5	C IV	1549	3.607
		7420.4	1.7
		9003.4	2.9
		9153.0	2.7
PSS J0133+0400	4.154	6293.6	1.9	Si II	1260	3.993
		6320.8	5.6	C IV	1548	3.083
		6349.0	4.8	Fe II	2383	1.665
		6367.7	6.4	C II	1334	3.771
		6403.4	2.9	C IV	1548	3.136
		6414.0	1.4	C IV	1551	3.136
		6437.7	1.6	Si IV	1393	3.619
		6476.7	1.4	Si IV	1402	3.617
		6503.1	2.1	O I	1302	3.994
		6649.5	2.4	Si IV	1393	3.771
		6665.8	2.6
		6694.3	1.5	Si IV	1402	3.772
		6891.3	2.2	Fe II	2586	1.664
		6963.1	3.8	Si IV	1393	3.996
		7001.9	2.5	Si IV	1402	3.991
		7128.9	3.2
		7149.5	2.3	C IV	1548	3.618
		7162.3	1.9	C IV	1551	3.619
		...	or	Si II	1527	3.691
		7176.0	0.9
		7214.8	0.9
		7284.1	4.3	Si II	1527	3.771
		7385.7	3.5	Si II	1808	3.085
		7450.1	4.6	Mg II	2796	1.664
		7469.4	4.4	Mg II	2803	1.664
		7599.2	4.3	Mg I	2853	1.664
		7623.1	1.7	Si II	1527	3.993
		7672.9	3.7	Fe II	1608	3.770
		7836.7	0.9	Al II	1671	3.690
		7855.1	1.1
		7919.3	5.5	C IV	1548	4.115
		7933.0	3.1	C IV	1551	4.116
		7971.6	4.7	Al II	1671	3.771
		8070.1	0.9
		8085.7	2.3
		8105.5	1.4
PSS J0134+3307	4.532	6744.5	1.9
		6834.8	2.2
		6856.5	1.4
		7129.4	1.2	Fe II	2586	1.756
		7166.4	2.3	Fe II	2600	1.756
		7255.3	2.9	C IV	1548	3.686
		7267.9	1.8	Si II	1527	3.761
		...	or	C IV	1551	3.686
		7391.9	1.8	C IV	1548	3.775
		7404.8	1.4	C IV	1551	3.775
		7689.0	1.4	Al II	1671	3.780
		7706.2	4.0	Mg II	2796	1.756

TABLE 7—Continued

Quasar	z_{em}	λ_{obs} (Å)	W_{obs} (Å)	Ion	λ_{rest} (Å)	z
		7727.6	3.2	Mg II	2803	1.756
		7861.0	1.2	Mg I	2853	1.755
		8198.2	0.7
		8280.7	2.7	Mg II	2796	1.961
		8300.7	2.0	Mg II	2803	1.961
		8340.0	0.6
		8537.7	3.9	C IV	1548	4.515
		8552.5	3.3	C IV	1551	4.515
PSS J0152+0735	4.051	6304.2	2.5	O I	1302	3.841
		6462.3	0.5	C II	1334	3.842
		6770.3	2.9	Fe II	2344	1.888
		6858.9	3.5	Fe II	2374	1.888
		6882.4	4.6	Fe II	2383	1.888
		7093.9	1.3
		7445.3	2.4
		7473.3	4.4	Fe II	2586	1.888
		7512.8	3.8	Fe II	2600	1.888
		7685.4	0.8
		8061.1	5.3	Mg II	2796	1.883
		8080.0	5.3	Mg II	2803	1.882
		8208.5	0.8
PSS J0209+0517	4.174	6330.9	0.9	Si II	1304	3.854
		6377.3	3.7	Mg II	2796	1.281
		6393.0	2.6	Mg II	2803	1.280
		6488.5	1.1	C II	1334	3.862
		6501.8	1.6	Mg I	2853	1.279
		6510.4	1.1
		6614.7	0.8
		6628.1	0.8
		6654.5	0.8
		6673.5	0.9
		6770.6	0.9
		6869.1	1.2
		7134.6	1.2	C IV	1548	3.608
		...	or	Si II	1527	3.673
		7145.9	0.7	C IV	1551	3.608
		7793.3	1.3	Al II	1671	3.664
		8123.6	1.9
SDSS J0211–0009	4.874	7199.9	1.3	C IV	1548	3.651
		7211.9	1.1	C IV	1551	3.651
		7227.4	4.3
		7262.9	2.2
		7411.0	2.4
		8122.3	4.2
		8618.6	0.0	Si II	1527	4.645
BR J0234–1806	4.301	6540.0	0.9	Si IV	1393	3.692
		6587.0	4.5	Si IV	1402	3.696
		6661.3	1.4
		6805.9	1.4	C IV	1548	3.396
		6818.3	1.5	C IV	1551	3.397
		6899.9	1.5
		6975.0	4.3

TABLE 7—*Continued*

Quasar	z_{em}	λ_{obs} (Å)	W_{obs} (Å)	Ion	λ_{rest} (Å)	z
		7138.7	1.5
		7161.5	2.3
		7282.3	2.1
		7401.0	1.7	C IV	1548	3.780
		7413.2	1.2	C IV	1551	3.780
		7840.1	1.7	Al II	1671	3.692
		7956.1	2.0
		7980.3	2.1
		8092.6	3.8	C IV	1548	4.227
		8107.9	1.8	C IV	1551	4.228
		8260.8	2.1
		8356.2	3.7
		8732.8	4.4
PSS J0248+1802	4.422	6682.8	0.3
		6865.3	0.4	Si IV	1393	3.926
		6885.0	0.8	Si IV	1393	3.939
		6910.3	0.6	Si IV	1402	3.926
		6928.5	0.8	Si IV	1402	3.939
		7184.1	0.4
		7646.1	2.8	C IV	1548	3.939
		7660.7	1.2	C IV	1551	3.940
		7788.9	1.1
BR J0301–5537	4.133	6278.7	3.2	C II	1334	3.705
		6357.7	1.0
		6409.2	0.8
		6421.9	0.9
		6442.2	0.9	Si II	1527	3.220
		6483.5	1.3
		6544.2	0.5
		6660.6	1.2
		6681.6	0.9	Si II	1527	3.377
		6970.3	2.2
		6999.3	1.3
		7219.3	0.5
		7281.2	1.7	C IV	1549	3.701
		7813.6	1.7
		8216.8	2.7
		8624.8	1.7
		8807.5	4.9
		8954.4	5.8
BR J0307–4945	4.728	7105.0	0.9
		7117.0	2.8	O I	1302	4.465
		7129.6	2.3	Si II	1304	4.466
		7224.0	1.2	C IV	1548	3.666
		7235.6	0.8	C IV	1551	3.666
		7261.9	4.2	Si IV	1393	4.210
		7271.9	2.8	Si IV	1393	4.217
		7293.8	4.0	C II	1334	4.465
		7308.4	3.1	Si IV	1402	4.210
		7318.3	1.0	Si IV	1402	4.217
		7382.6	0.7
		7469.2	1.1	C IV	1548	3.824

TABLE 7—Continued

Quasar	z_{em}	λ_{obs} (Å)	W_{obs} (Å)	Ion	λ_{rest} (Å)	z
		7482.4	0.7	C IV	1551	3.825
		7615.2	8.4	Si IV	1393	4.464
		7667.2	4.0	Si IV	1402	4.466
		7961.3	2.3
		8067.0	2.6	C IV	1548	4.210
		8077.9	3.6	C IV	1551	4.210
		...	and	C IV	1548	4.217
		8091.0	2.4	C IV	1551	4.217
		8180.1	2.0
		8345.0	2.8	Si II	1527	4.466
		8459.7	2.3	C IV	1548	4.464
		8473.2	1.2	C IV	1551	4.464
		8509.3	1.5
		8645.0	2.2
		8791.5	1.1	Fe II	1608	4.466
		8890.3	1.2
		8990.0	1.4
		9132.9	3.4	Al II	1671	4.466
		9155.4	1.7
		9175.6	1.9
SDSS J0310–0014	4.658	6921.0	7.1	Mg II	2796	1.475
		6939.6	4.1	Mg II	2803	1.475
		6955.3	4.6	O I	1302	4.341
		6976.8	3.2
		7049.2	3.6
		7126.0	1.6	C II	1334	4.340
		7391.4	3.5	Al II	1671	3.424
		7467.5	4.1
		7706.3	0.0
		8229.9	3.6
		8655.0	0.0
		9086.7	6.9
BR J0311–1722	4.039	6163.0	0.6	O I	1302	3.733
		6173.3	0.8	Si II	1304	3.733
		6316.0	1.0	C II	1334	3.733
		6379.3	2.2
		6421.2	0.5
		6464.8	1.1
		6476.3	0.9
		6489.7	2.1
		6767.5	1.6
		7006.4	1.1	Fe II	2383	1.940
		7078.6	1.0
		7087.8	0.9
		7138.3	0.9
		7645.6	1.9	Fe II	2600	1.940
		7794.7	4.6	Mg II	2796	1.787
		7810.0	3.1	Mg II	2803	1.786
		8220.9	4.0	Mg II	2796	1.940
		8241.4	1.9	Mg II	2803	1.940
BR J0324–2918	4.622	6899.4	1.2
		6987.6	0.6

TABLE 7—Continued

Quasar	z_{em}	λ_{obs} (Å)	W_{obs} (Å)	Ion	λ_{rest} (Å)	z
		7098.6	2.5	C IV	1548	3.585
		7110.7	1.4	C IV	1551	3.585
		7137.8	1.7
		7206.6	0.8
		7416.9	1.8
		7454.7	0.6
		7483.8	0.8
		7528.6	0.6
		7643.4	1.1	Fe II	2367	2.228
		7692.4	1.1	Fe II	2383	2.228
		7874.3	1.1
		8064.1	1.1
		8179.5	0.8
		8291.6	1.2	Si II	1808	3.586
		8349.7	1.1	Fe II	2586	2.228
		8391.9	1.5	Fe II	2600	2.227
		8542.8	1.0
		8624.3	3.4
		9026.9	2.6	Mg II	2796	2.228
		9050.4	1.4	Mg II	2803	2.228
		9062.7	1.2
		9131.6	1.2
BR J0334–1612	4.363	6560.8	1.4
		6957.9	4.9	Si II	1527	3.558
		7284.8	2.3	C IV	1548	3.705
		7295.2	2.5	C IV	1551	3.704
		7364.7	2.2	C IV	1548	3.757
		7375.2	2.4	C IV	1551	3.756
		7667.6	6.9
		7682.5	2.9
		7698.1	8.4
		7737.2	6.6
		7825.1	5.8
SDSS J0338+0021	5.010	7323.1	1.8
		7722.9	4.9	Si II	1527	4.059
		7756.8	3.5
		8352.1	3.9
		8466.5	5.5	Al II	1671	4.067
BR J0355–3811	4.545	6776.8	1.8	C IV	1548	3.377
		6787.0	1.4	C IV	1551	3.377
		6858.1	0.5
		6871.2	0.5
		6960.1	3.2
		6997.4	4.6	Fe II	2344	1.985
		7091.0	1.0	Fe II	2374	1.986
		7116.9	4.9	Fe II	2383	1.987
		7223.9	1.0
		7414.2	0.8	Si IV	1393	4.319
		7464.1	1.2	Si IV	1402	4.321
		7695.6	1.3
		7723.5	2.1	Fe II	2586	1.986
		7746.1	0.6

TABLE 7—Continued

Quasar	z_{em}	λ_{obs} (Å)	W_{obs} (Å)	Ion	λ_{rest} (Å)	z
		7765.5	4.1	Fe II	2600	1.987
		7799.3	1.6
		8237.6	1.3	C IV	1548	4.321
		8250.7	0.7	C IV	1551	4.320
		8296.7	1.5	C IV	1548	4.359
		8309.9	1.6	C IV	1551	4.359
		8350.7	10.5	Mg II	2796	1.986
		8372.4	8.9	Mg II	2803	1.986
		8488.1	0.5
		8519.4	1.1	Mg I	2853	1.986
		8552.6	2.2	C IV	1548	4.524
		8568.7	1.3	C IV	1551	4.525
		8739.8	1.1
		8797.4	9.4
		8911.2	5.0
		8941.6	10.8
BR J0403–1703	4.227	7897.6	10.4
		7932.8	10.6
		8112.9	2.3
		8303.2	10.2
BR J0415–4357	4.070	6236.6	2.1
		6257.8	5.1	O I	1302	3.806
		6268.4	6.5	Si II	1304	3.806
		6286.2	4.6
		6413.6	3.5	C II	1334	3.806
		7012.8	1.4
		7339.6	2.6	Si II	1527	3.808
		7782.0	1.4
		7793.9	3.4
		7831.6	5.8	C IV	1548	4.059
		7844.5	5.5	C IV	1551	4.058
BR J0419–5716	4.461	6728.3	0.5
		6843.6	1.6
		7013.9	2.1	Mg II	2796	1.508
		7031.7	1.6	Mg II	2803	1.508
		7103.6	1.3	Fe II	2344	2.030
		7221.0	2.1	Fe II	2383	2.031
		7375.8	1.0
		7527.8	0.7
		7878.2	2.6	Fe II	2600	2.030
		8080.3	2.4
		8181.1	0.7
		8417.9	1.4
		8438.6	1.3
		8474.0	5.2	Mg II	2796	2.030
		8494.9	3.4	Mg II	2853	2.030
		8582.6	6.6
		8953.4	4.2
BR J0426–2202	4.320	6652.8	0.6	Al II	1671	2.982
		6767.4	1.1
		7031.4	1.8
		7134.9	4.1	C IV	1548	3.609

TABLE 7—Continued

Quasar	z_{em}	λ_{obs} (Å)	W_{obs} (Å)	Ion	λ_{rest} (Å)	z
		7147.0	1.4	C IV	1551	3.609
		7210.9	2.1	Si IV	1393	4.174
		7257.3	1.2	Si IV	1402	4.174
		8010.9	2.5	C IV	1548	4.174
		8024.2	2.1	C IV	1551	4.174
		8278.1	1.8
		8291.4	1.0
		8405.5	0.9
		9001.4	1.4	Fe II	2260	2.982
		9024.2	1.3
PMN J0525–3343	4.383	6604.0	7.8
		6682.0	0.7	Fe II	2600	1.570
		6728.8	6.0
		7185.3	2.2	Mg II	2796	1.570
		7204.1	2.2	Mg II	2853	1.570
		7223.9	0.8
		7470.2	0.5
		7482.4	1.5
		7500.1	0.7
		7529.2	0.3
		7572.5	2.8
		7667.8	1.0
		7759.3	1.8
		7776.4	0.0	Fe II	2586	2.006
		7803.2	1.5
		7845.6	0.9
		7952.3	1.5
		8409.7	7.1	Mg II	2796	2.007
		8425.0	6.3	Mg II	2796	2.005
BR J0529–3526	4.413	6685.9	0.5
		6952.1	1.2
		7355.6	1.8	Fe II	1608	3.573
		7637.5	2.4	Al II	1671	3.571
BR J0529–3552	4.172	6527.2	1.1
		6567.7	3.6
		6608.7	0.7	Si II	1304	4.067
		6856.2	0.7
		6962.2	1.3	C IV	1548	3.497
		6975.0	2.1	C IV	1551	3.498
		7060.3	0.8	Si IV	1393	4.066
		7106.0	1.1	Si IV	1402	4.066
		7224.0	1.1
		7290.1	2.1
		7432.6	0.9	Mg II	2796	1.658
		7450.4	1.2	Mg II	2803	1.658
		7501.0	0.7
		7890.2	3.7	Si II	1526	4.168
		7993.6	1.3	C IV	1548	4.163
		8003.7	1.4	C IV	1551	4.161
BR J0714–6455	4.462	6717.3	0.7
		6845.4	0.6
		6926.2	0.8

TABLE 7—Continued

Quasar	z_{em}	λ_{obs} (Å)	W_{obs} (Å)	Ion	λ_{rest} (Å)	z
		7222.3	0.4
		7346.6	0.6	C IV	1548	3.745
		7356.3	1.5	C IV	1551	3.744
		...	or	C IV	1548	3.752
		7367.8	0.9	C IV	1551	3.751
		7654.7	1.9
		7694.2	2.2	C IV	1548	3.970
		7707.5	1.7	C IV	1551	3.970
		8044.3	2.1	C IV	1548	4.196
		8060.1	1.8	C IV	1551	4.197
		8242.5	0.9
		8984.7	5.0
PSS J0747+4434	4.430	6698.9	2.5	C II	1334	4.020
		7024.8	0.8
		7151.3	7.0
		7166.6	3.8
		7636.8	2.4
		8288.5	1.8
		8382.5	1.1	Al II	1671	4.017
RX J1028–0844	4.276	6463.8	2.0
		6551.4	1.4
		6697.4	1.0
		6709.3	1.2
		6751.8	1.2	Si II	1527	3.423
		6967.4	1.3
		7040.3	1.4	Fe II	2383	1.955
		7179.9	2.2
		7227.2	0.5
		7235.8	0.6
		7388.0	1.4	Al II	1671	3.422
		7682.1	1.3	Fe II	2600	1.954
		7737.0	2.5	C IV	1548	3.997
		7749.1	3.4	C IV	1551	3.997
		7777.1	1.3
		8261.2	4.4	Mg II	2796	1.954
		8280.4	2.4	Mg II	2803	1.954
		8432.9	3.0	Mg I	2853	1.956
		...	or	Al II	1671	4.047
PSS J1057+4555	4.116	6315.9	1.4	Si IV	1393	3.532
		6356.8	1.1	Si IV	1402	3.532
		6452.5	1.7
		6532.0	4.2	Fe II	1608	3.061
		6559.8	2.4	C IV	1548	3.237
		6571.1	1.3	C IV	1551	3.237
		6589.1	0.8	Si II	1527	3.316
		6672.6	4.0	Mg II	2796	1.386
		6688.5	3.8	Mg II	2803	1.386
		6724.3	1.3
		6768.5	0.5	Al II	1671	3.051
		6806.3	0.4	Mg I	2853	1.386
		6875.2	0.6
		7018.1	4.0	C IV	1549	3.531

TABLE 7—*Continued*

Quasar	z_{em}	λ_{obs} (Å)	W_{obs} (Å)	Ion	λ_{rest} (Å)	z
		7180.3	0.6
		7197.5	0.2
		7212.1	0.3	Al II	1671	3.317
		7251.4	1.9	Si II	1526	3.750
		7283.7	1.0	Fe II	1608	3.529
		7320.6	0.3	Si II	1808	3.049
		7358.7	1.0	C IV	1548	3.753
		7371.1	0.5	C IV	1551	3.753
		7469.9	1.9	C IV	1548	3.825
		7482.2	0.8	C IV	1551	3.825
		7574.0	0.5	Al II	1671	3.533
		7635.5	1.6	C IV	1548	3.932
		7649.2	0.7	C IV	1551	3.933
		7699.2	0.4
		8414.7	1.7
PSS J1159+1337	4.073	6222.7	0.3
		6271.6	1.6
		6292.1	0.7
		6302.9	2.4	C II	1334	3.723
		6419.2	1.3	Fe II	2344	1.738
		6524.0	1.9	Fe II	2383	1.738
		6584.6	1.7	Si IV	1393	3.724
		6625.1	0.9	Si IV	1402	3.723
		6877.2	1.2	Mg II	2796	1.459
		6893.6	0.6	Mg II	2803	1.459
		6956.8	0.4
		7082.6	1.0	Fe II	2586	1.738
		7120.0	1.5	Fe II	2600	1.738
		7211.2	0.7	Si II	1527	3.723
		7248.6	0.4
		7313.5	1.2	C IV	1548	3.724
		7325.4	0.6	C IV	1551	3.724
		7537.3	0.3
		7637.4	1.6
		7656.3	5.4	Mg II	2796	1.738
		7676.9	3.7	Mg II	2803	1.738
		7816.7	0.8	Mg I	2853	1.740
		7839.1	1.8	C IV	1548	4.063
		7853.3	1.0	C IV	1551	4.064
		7891.8	1.5	Al II	1671	3.723
		7904.7	0.3
		8142.6	0.4
		8232.7	0.4
		8259.0	0.3
PSS J1253+0228	4.007	6142.0	2.2	C II	1334	3.602
		6317.2	1.9	Al II	1671	2.781
		6415.0	4.8	Si IV	1402	3.603
		6455.0	3.8	Si IV	1527	3.602
		7125.4	5.5	C IV	1548	3.602
		7137.3	4.1	C IV	1551	3.602
		7277.8	1.0
		7396.5	1.4	Fe II	1608	3.599

TABLE 7—Continued

Quasar	z_{em}	λ_{obs} (Å)	W_{obs} (Å)	Ion	λ_{rest} (Å)	z
		7725.6	3.5	C IV	1548	3.990
		7738.9	1.4	C IV	1551	3.990
		7854.3	1.2
		7880.5	2.5
		7918.5	0.7
		8034.2	3.1	Fe II	1608	3.995
		8073.6	1.8
BR J1310–1740	4.185	6352.6	1.4
		6409.3	1.2
		6477.9	2.2	Mg II	2796	1.317
		6496.4	2.0	Mg II	2803	1.317
		6770.2	1.7	Si II	1527	3.435
		6864.3	5.7	C IV	1548	3.434
		6875.2	4.3	C IV	1551	3.433
		7189.0	1.2
		7279.6	0.9
		7406.9	3.2	Al II	1671	3.433
		7644.7	3.2
		7752.6	1.3
		7826.1	1.5
		7894.4	2.6
		7933.8	3.1
		7981.6	1.2	C IV	1548	4.155
		7995.4	1.2	C IV	1551	4.156
		8298.0	1.5
		8346.3	2.8
BR J1330–2522	3.949	6013.0	3.4
		6051.0	12.4
		6077.4	8.7
		6231.3	1.5	Si II	1527	3.082
		6303.3	3.3
		6317.6	3.7	C IV	1548	3.081
		6329.4	1.9	C IV	1551	3.081
		6393.7	1.9
		6561.7	1.1	Fe II	1608	3.080
		6816.8	1.0	Al II	1671	3.080
		6875.6	1.9	Si IV	1393	3.933
		6921.0	1.1	Si IV	1402	3.934
		7288.0	1.1
		7304.5	1.1
		7381.5	1.7	C IV	1548	3.768
		7394.0	1.2	C IV	1551	3.768
		7438.9	1.4
		7459.1	1.4
		7568.6	3.7	C IV	1548	3.889
		7582.2	2.9	C IV	1551	3.889
		7656.1	1.0
		8348.0	1.6
		8435.9	1.6
FIRST J1410+3409	4.351	6528.0	3.5
		6577.6	8.2
		6873.8	5.4

TABLE 7—Continued

Quasar	z_{em}	λ_{obs} (Å)	W_{obs} (Å)	Ion	λ_{rest} (Å)	z
PSS 1456+2007	4.249	7311.7	7.3
		8347.1	9.4
		6373.0	8.9
		6447.5	0.5	Si II	1527	3.223
		6928.9	2.1	Si IV	1393	3.971
		6972.2	1.8	Si IV	1402	3.970
		7150.8	1.8
		7232.5	2.4
		7273.7	2.6
		7449.2	1.7
		7465.7	1.9
		7631.4	1.4	Si II	1808	3.221
		7753.8	2.1
		7977.5	1.4
BR J1603+0721	4.385	8401.5	3.0
		6604.4	0.8
		6730.1	2.1
		6801.5	3.1
		6813.7	1.6
		6876.0	2.1
		6898.6	1.5
		7634.3	1.4	C IV	1548	3.931
		7645.5	0.7	C IV	1551	3.930
		7753.1	2.0	C IV	1548	4.008
		7766.2	1.5	C IV	1551	4.008
		8233.0	1.8	C IV	1548	4.318
		8246.5	1.0	C IV	1551	4.317
PSS J1618+4125	4.213	6561.1	2.2
		6857.1	5.1	Si IV	1393	3.920
		7058.5	1.7
		7378.5	5.5
		7502.6	6.2	Si II	1527	3.914
		7522.2	3.1
		7855.7	3.0
		7986.1	3.7
		8027.3	1.6
		8186.1	4.7
PSS J1633+1411	4.351	6542.7	1.8
		6564.7	2.0
		6625.1	0.4
		6728.1	0.5
		6833.1	0.3
		6972.5	2.6	C IV	1548	3.504
		6983.7	1.7	C IV	1551	3.503
		7178.4	0.6
		7227.2	0.9
		7325.1	0.6	Si IV	1393	4.256
		7371.9	0.6	Si IV	1402	4.255
		7577.9	1.0	C IV	1548	3.895
		7591.0	0.5	C IV	1551	3.895
		7703.3	1.6	C IV	1548	3.976
		7717.1	0.7	C IV	1551	3.976

TABLE 7—Continued

Quasar	z_{em}	λ_{obs} (Å)	W_{obs} (Å)	Ion	λ_{rest} (Å)	z
		7890.3	0.8	Fe II	1608	3.906
		7930.1	1.1
		8102.6	1.2
		8138.0	2.2	C IV	1548	4.256
		8148.9	1.7	C IV	1551	4.255
		8178.0	1.4
		8217.4	0.8
		8230.3	0.5
		8299.6	3.4
PSS J1646+5514	4.037	6335.9	1.7
		6490.6	0.4	C IV	1548	3.192
		6502.1	0.2	C IV	1551	3.193
		6549.7	0.5
		6624.5	0.2
		6638.2	0.4	C IV	1548	3.288
		6649.1	0.2	C IV	1551	3.288
		6712.2	0.9
		6857.5	0.3
		6870.7	0.5
		6891.3	0.2	Si IV	1402	3.913
		7010.8	0.9	Si IV	1393	4.030
		7033.0	2.1	C IV	1548	3.543
		7044.9	1.3	C IV	1551	3.543
		7055.6	0.4	Si IV	1402	4.030
		7356.8	1.2	C IV	1548	3.752
		7368.2	0.7	C IV	1551	3.751
		7678.4	0.5
		7785.2	1.9	C IV	1548	4.029
		7799.2	1.6	C IV	1551	4.029
		7955.2	0.2
		7993.1	0.6	Mg II	2796	1.858
		8013.7	0.2	Mg II	2803	1.858
		8404.5	0.9
PSS J1721+3256	4.031	6486.1	1.2	Fe II	2586	1.508
		6518.9	1.5	Fe II	2600	1.507
		6568.3	1.5
		6727.6	1.6	C IV	1548	3.345
		6738.6	0.8	C IV	1551	3.345
		7008.2	5.3	Mg II	2796	1.506
		7026.4	1.7	Mg II	2803	1.506
		7291.9	1.8	C IV	1548	3.710
		7305.3	0.8	C IV	1551	3.711
RX J1759+6638	4.320	6561.7	2.5	Mg II	2796	1.347
		6579.2	1.7	Mg II	2803	1.347
		6643.1	0.6
		6715.0	1.3	Si II	1527	3.398
		6808.7	2.5	C IV	1548	3.398
		6817.2	2.0	C IV	1551	3.396
		6870.5	4.4
		7319.6	2.6
		7345.7	2.7	Al II	1671	3.397
		7752.8	2.7

TABLE 7—Continued

Quasar	z_{em}	λ_{obs} (Å)	W_{obs} (Å)	Ion	λ_{rest} (Å)	z
PSS J1802+5616	2.891	8347.1	5.6	C IV	1548	4.391
		8359.9	3.1	C IV	1551	4.391
		6336.2	6.2
		6414.8	0.8	C II	1334	3.807
		6454.1	1.2
		6619.4	2.1
		6696.2	3.9	Si II	1527	3.386
		6798.8	2.3	C IV	1549	3.389
		6868.9	2.7
		6945.7	2.9
PSS J2122–0014	4.114	6300.7	1.5	Si II	1260	3.999
		6353.1	4.1	C IV	1548	3.104
		6363.2	3.3	C IV	1551	3.103
		6373.8	3.7	C IV	1548	3.117
		6384.5	2.4	C IV	1551	3.117
		6421.4	2.5	Si II	1527	3.206
		6511.4	0.8	C IV	1548	3.206
		6522.6	0.5	C IV	1551	3.206
		6570.3	5.1	C IV	1548	3.244
		6581.8	4.1	C IV	1551	3.244
		6600.7	1.7	C IV	1548	3.264
		6611.8	1.0	C IV	1551	3.264
		6763.7	0.7	Fe II	1608	3.205
		6952.9	2.2
		6967.2	2.5
		7026.7	1.7	Al II	1671	3.206
		7094.2	1.9
		7147.7	2.6	Si IV	1393	4.128
PMN J2134–0419	4.334	7194.9	2.0	Si IV	1402	4.129
		7225.1	7.2	C IV	1549	3.664
		7321.5	7.6	C IV	1549	3.727
		7400.9	22.4	C IV	1549	3.778
		7634.9	1.3	Si II	1527	4.001
		7708.8	1.2
		7741.0	1.9	C IV	1548	4.000
		7754.9	1.1	C IV	1551	4.001
		7870.4	1.0
		7879.1	0.7
8083.7	4.334	7890.4	1.1
		7939.0	5.0	C IV	1548	4.128
		7952.0	5.9	C IV	1551	4.128
		6599.0	1.5	C IV	1548	3.262
		6607.9	0.5	C IV	1551	3.261
		6646.6	2.1
		6770.2	0.8
		6849.4	2.2
8227.1	4.334	6865.4	2.4	Fe II	1608	3.269
		7873.0	2.6
		8083.7	2.4
		8227.1	1.8

TABLE 7—Continued

Quasar	z_{em}	λ_{obs} (Å)	W_{obs} (Å)	Ion	λ_{rest} (Å)	z
PSS J2154+0335	4.363	6548.0	0.7	Fe II	2374	1.758
		6570.4	2.8	Fe II	2383	1.757
		6627.3	1.5
		6640.6	2.2
		6873.2	3.0
		6889.1	2.2
		6916.1	1.4
		7057.3	0.7	Si II	1527	3.623
		7133.6	1.9	Fe II	2586	1.758
		7170.3	2.8	Fe II	2600	1.758
		7397.1	3.9	C IV	1548	3.778
		7409.4	3.0	C IV	1551	3.778
PSS J2155+1358	4.256	6457.8	4.3
		6541.2	1.3	N V	1240	4.275
		6566.6	0.7
		6589.2	2.1	Si II	1527	3.316
		...	or	Fe II	2260	1.915
		6678.1	3.7	C IV	1549	3.311
		6710.8	0.6
		6785.2	0.6
		6811.2	0.9
		6830.6	0.9	Fe II	2344	1.914
		6890.9	0.5
		6916.9	0.9	Fe II	2374	1.913
		6941.7	2.9	Fe II	1608	3.316
		7066.2	1.9	C IV	1548	3.564
		7078.1	1.1	C IV	1551	3.564
		7133.7	0.8
		7170.5	4.5
		7207.6	2.8	Al II	1671	3.314
		7307.0	2.6	Si IV	1393	4.243
		7354.1	1.9	Si IV	1402	4.243
		7564.6	1.0
		7577.9	1.7	Fe II	2600	1.914
		7877.8	1.6
		7892.2	1.2
		7939.0	1.3
		7952.1	1.2
BR J2216−6714	4.469	8115.1	2.8	C IV	1548	4.242
		8129.6	1.8	C IV	1551	4.242
		8147.0	3.2	Mg II	2796	1.913
		8169.3	4.6	Mg II	2853	1.914
		8187.1	0.9
		9064.7	2.2
		9127.7	0.6
		6744.0	1.1
		6764.7	2.1	C IV	1548	3.369
		6776.4	0.3	C IV	1551	3.370
		6790.4	0.4
		6851.4	0.4	O I	1302	4.262
		6918.5	1.8	Fe II	2260	2.060
		6942.1	0.4

TABLE 7—Continued

Quasar	z_{em}	λ_{obs} (Å)	W_{obs} (Å)	Ion	λ_{rest} (Å)	z
		7003.8	0.9
		7068.2	1.4
		7137.1	0.6
		7175.7	2.7	Fe II	2344	2.061
		7203.5	1.3
		7267.8	2.9	Fe II	2374	2.061
		7293.8	4.5	Fe II	2383	2.061
		7889.8	2.0	Si II	1808	3.364
		7918.1	2.4	Fe II	2586	2.061
		7958.5	3.4	Fe II	2600	2.061
		8327.1	1.9
		8559.1	3.6	Mg II	2796	2.061
		8582.1	3.4	Mg II	2803	2.061
		8731.0	1.5	Mg I	2853	2.060
		9094.6	1.8
PSS J2241+1352	4.441	6738.7	0.8
		6752.2	3.4
		6810.4	1.2
		6833.8	1.3
		6878.1	3.7	O I	1302	4.282
		6892.0	3.4	Si II	1304	4.284
		6951.5	1.4
		7049.6	3.7	C II	1334	4.282
		7135.2	1.3
		7230.4	1.5
		7267.6	1.6
		7363.2	1.9
		7400.3	15.3	Si IV	1400	4.286
		8066.2	2.8	Si II	1527	4.283
		8307.0	2.3
		8344.5	3.7
		8401.2	3.2	Si II	1808	3.647
		8437.7	4.5	C IV	1549	4.447
		8499.1	3.8	Fe II	1608	4.284
		9210.7	4.7
BR J2317-4345	3.943	6049.4	1.3
		6136.0	0.5	Fe II	2260	1.714
		6248.8	3.6	Si IV	1393	3.483
		6290.6	0.5	Si IV	1402	3.484
		6362.4	0.6	Fe II	2344	1.714
		6466.9	1.4	Fe II	2382	1.714
		6553.4	0.7
		6702.1	0.9
		6809.5	0.8
		6944.6	3.8	C IV	1548	3.486
		6956.7	3.5	C IV	1551	3.486
		7057.8	1.5	Fe II	2600	1.714
		7084.1	2.7	C IV	1548	3.576
		7097.2	1.0	C IV	1551	3.577
		7224.3	0.8	Fe II	1608	3.491
		7590.2	2.6	Mg II	2796	1.714
		7609.1	2.8	Mg II	2803	1.714

TABLE 7—Continued

Quasar	z_{em}	λ_{obs} (Å)	W_{obs} (Å)	Ion	λ_{rest} (Å)	z
		7719.5	0.9
		7739.8	3.3	Mg I	2853	1.713
		7853.8	1.7
BR J2328–4513	4.359	6573.7	2.5	N V	1240	4.301
		6619.8	1.0
		6856.2	0.9
		6877.1	1.9	Fe II	2600	1.645
		7019.3	1.7
		7140.6	2.8
		7225.5	2.1
		7306.6	2.2	Si II	1808	3.041
		...	or	C IV	1548	3.719
		7319.2	1.0	C IV	1551	3.720
		7396.4	2.7	Mg II	2796	1.645
		7415.0	1.3	Mg II	2803	1.645
		7792.3	4.5	C IV	1548	4.033
		7804.9	2.2	C IV	1551	4.033
		8113.1	1.4
		8176.6	1.6
		8240.3	1.3
		8258.4	1.3
		8365.4	2.5
		8400.3	1.4
		8501.7	2.4
PSS J2344+0342	4.239	6515.2	2.9
		6531.4	2.8	C IV	1548	3.218
		6541.8	2.6	C IV	1551	3.218
		6650.1	0.9	Si II	1808	2.678
		6786.0	1.3	Fe II	1608	3.219
		6804.0	2.7	Si IV	1393	3.882
		6848.4	1.3	Si IV	1402	3.882
		6869.5	1.5
		7049.1	3.8	Al II	1671	3.219
		7200.8	1.2
		7236.8	2.0
		7326.9	1.5	Mg II	2796	1.620
		7347.3	2.2	Mg II	2803	1.621
		7453.1	0.7	Si II	1526	3.882
		7504.5	1.3
		7560.2	2.4
		7630.5	2.4	Si II	1808	3.220
		7775.9	0.8
		8153.9	2.9
		8329.9	1.7	Fe II	2260	2.684
		8436.2	3.1
		8466.4	4.5
		8707.9	1.8	Fe II	2367	2.678
BR J2349–3712	4.208	6423.7	0.8	N V	1240	4.169
		6398.2	1.2
		6437.5	1.8
		6477.0	0.9
		6592.6	1.3

TABLE 7—*Continued*

Quasar	z_{em}	λ_{obs} (Å)	W_{obs} (Å)	Ion	λ_{rest} (Å)	z
	6759.7	1.1
	6770.8	1.1
	7090.9	1.7
	7161.2	1.1	Si II	1527	3.691	
	7305.6	1.4
	7371.5	1.3
	7716.3	1.3
	8784.6	3.0
	9122.6	2.8

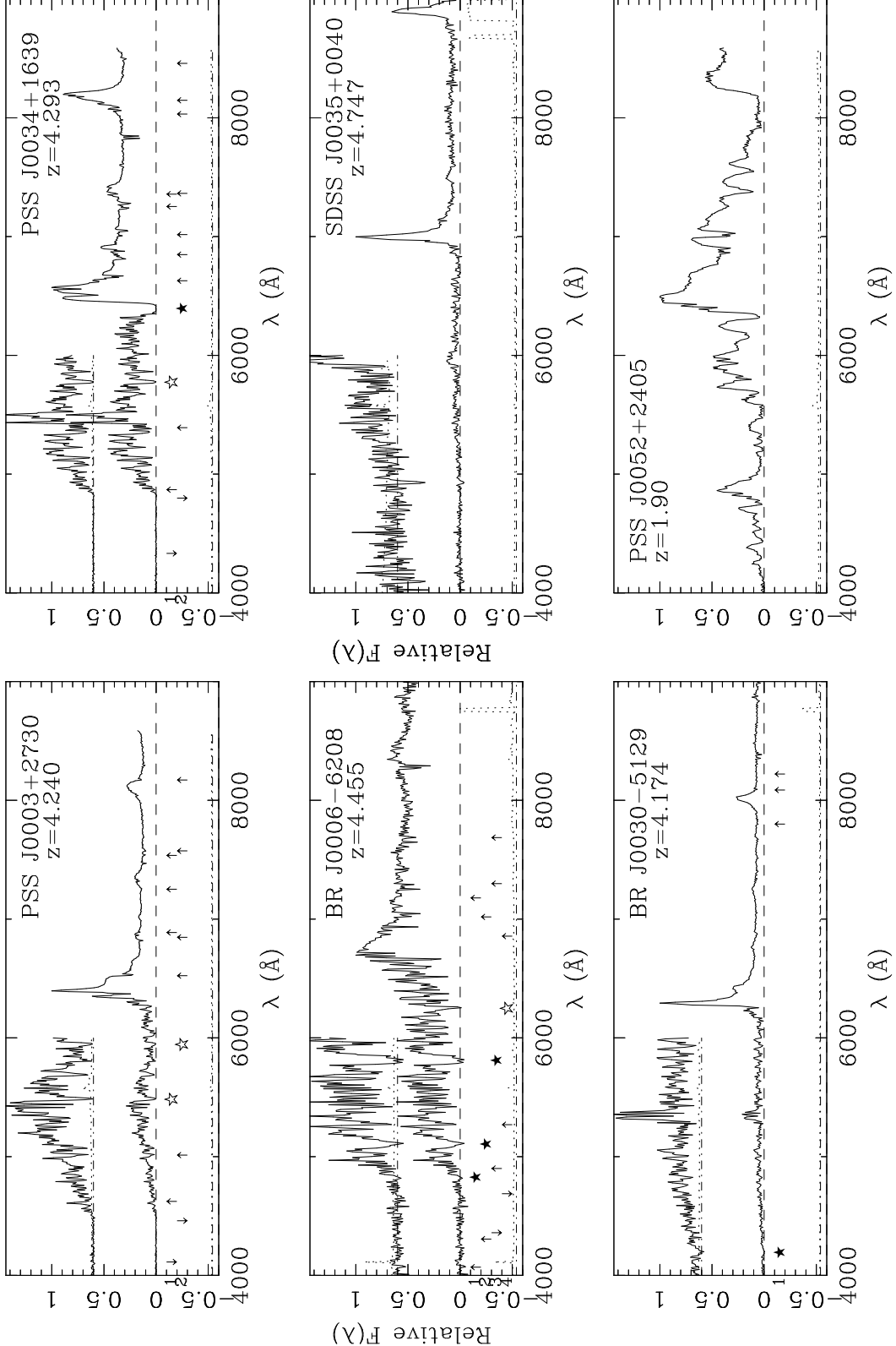
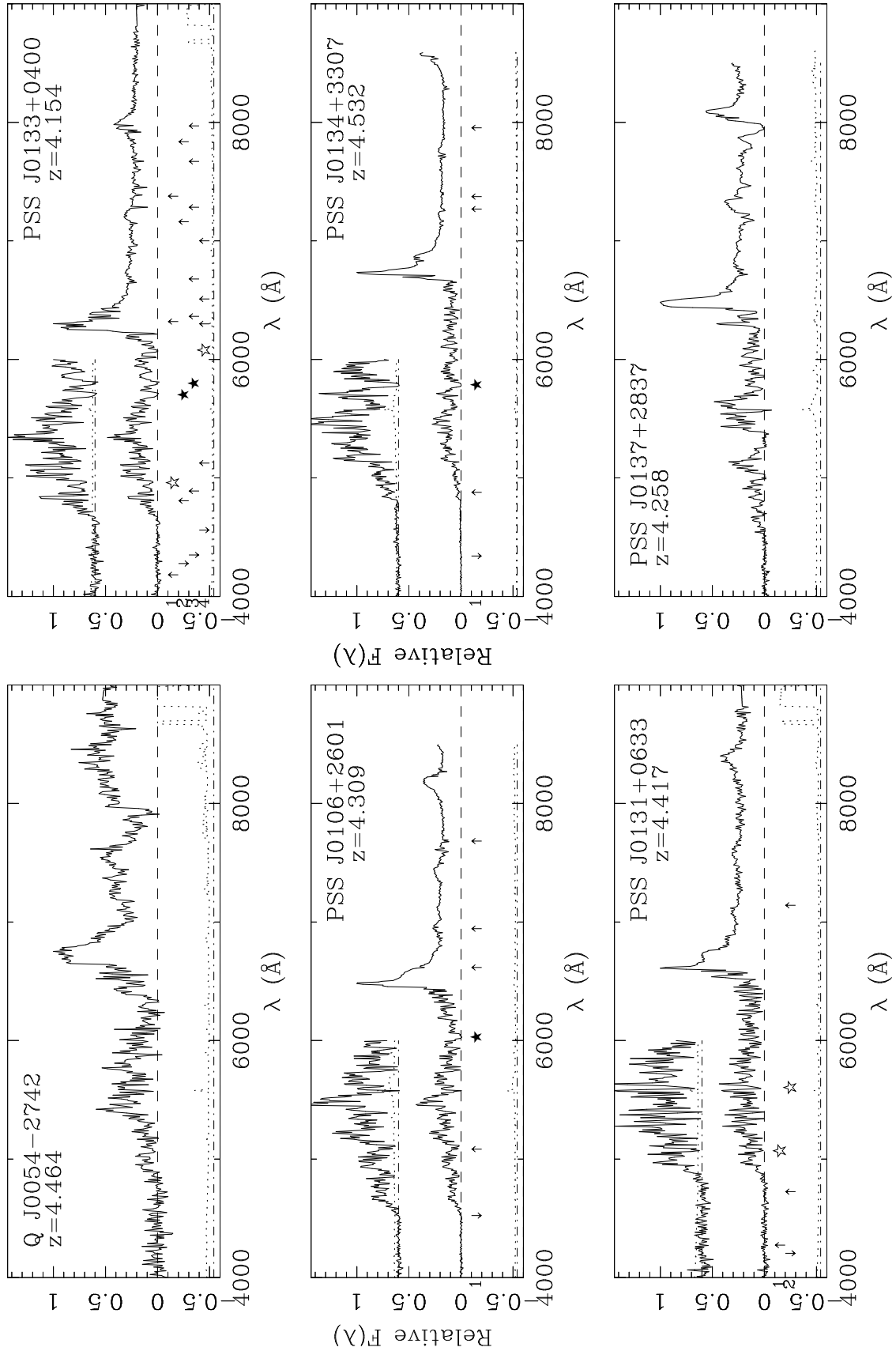
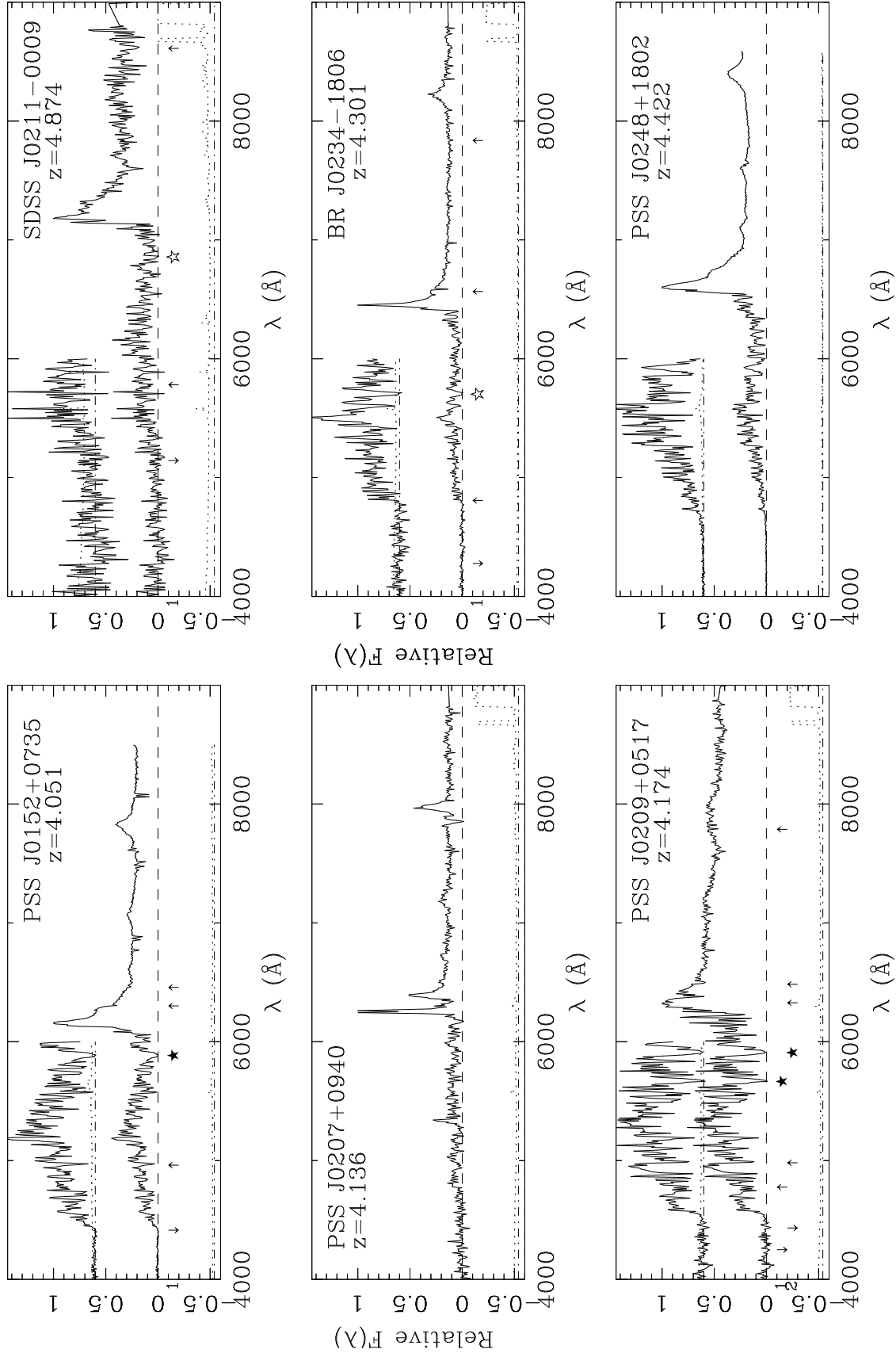
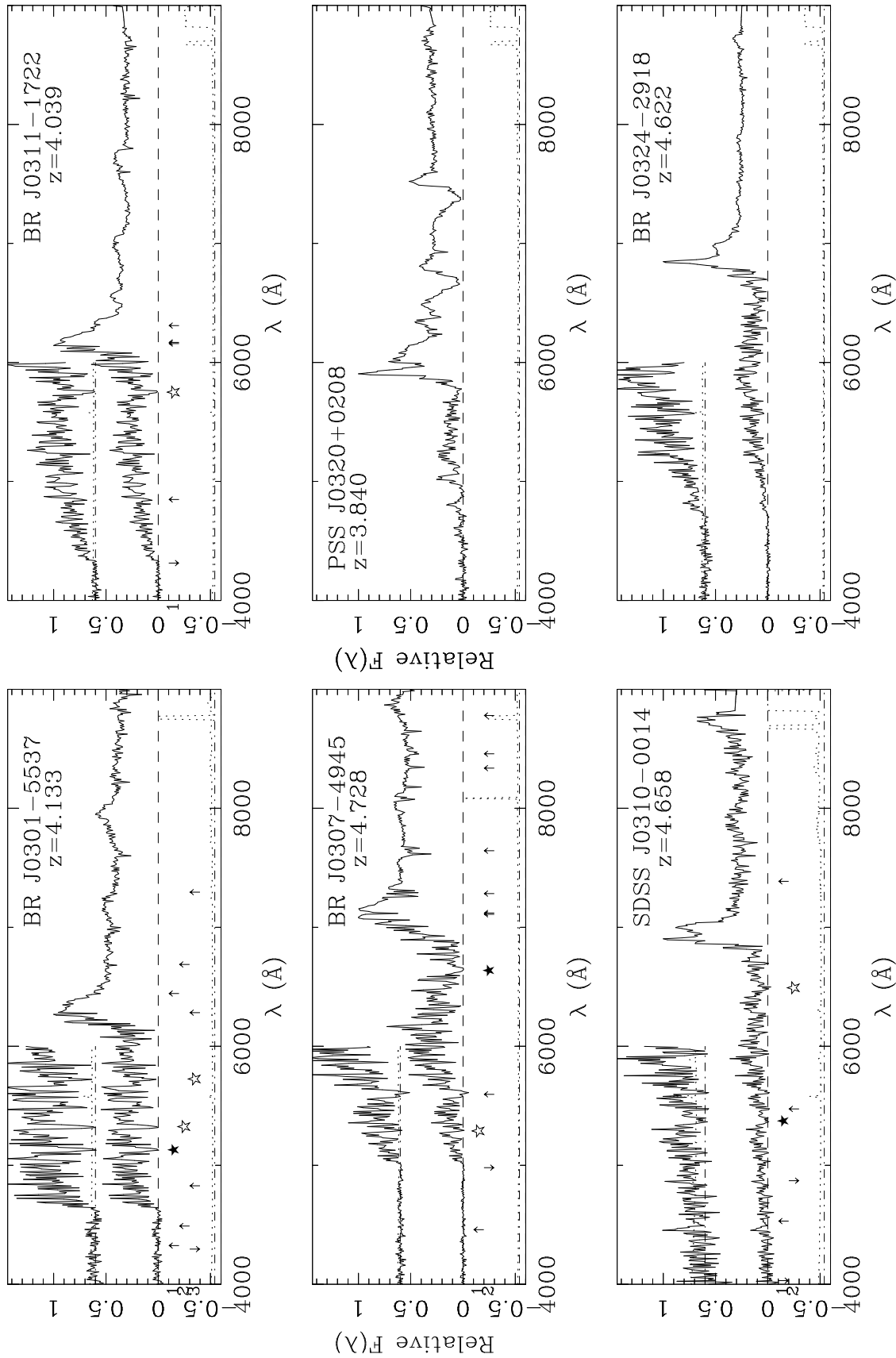
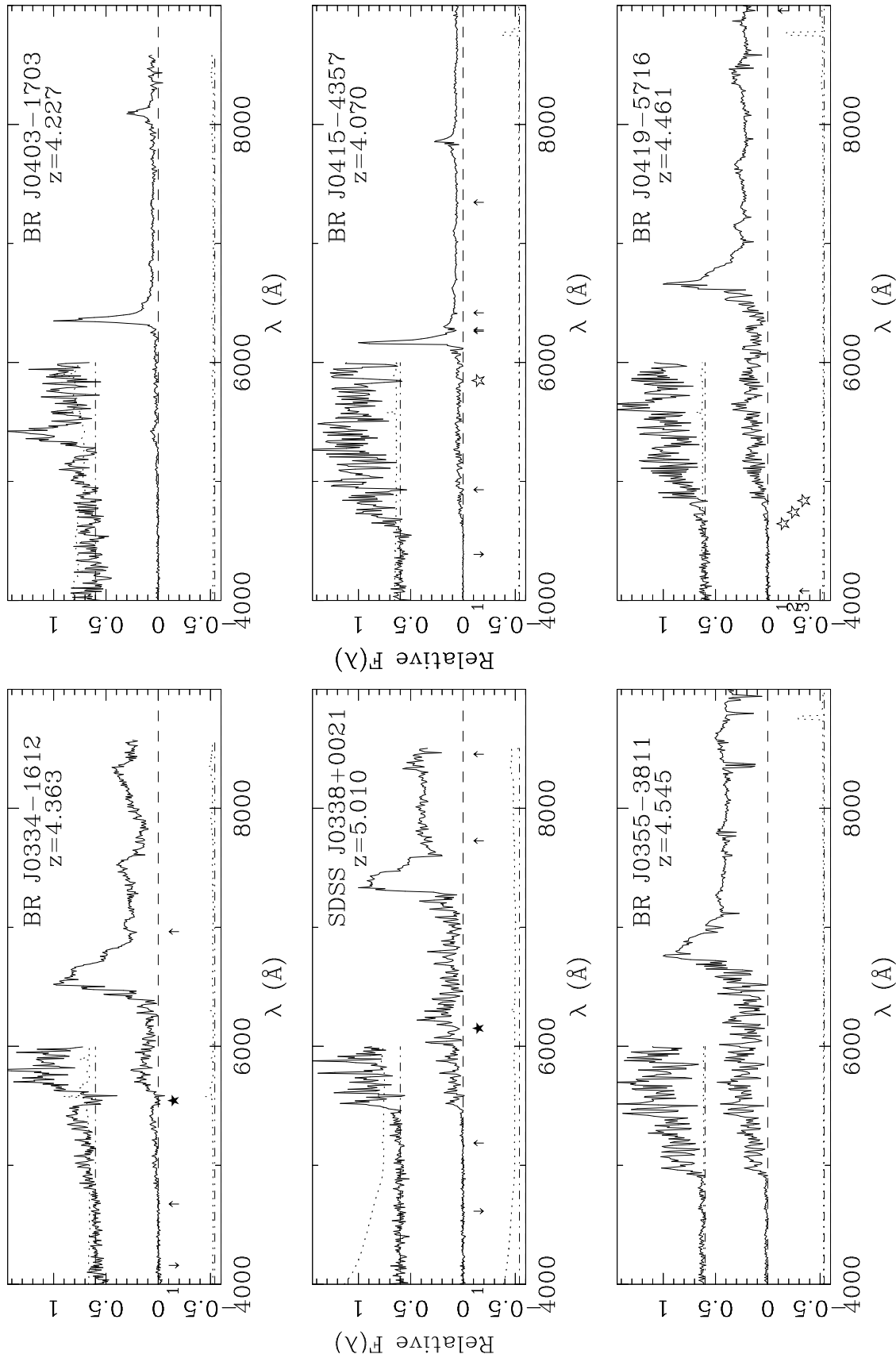


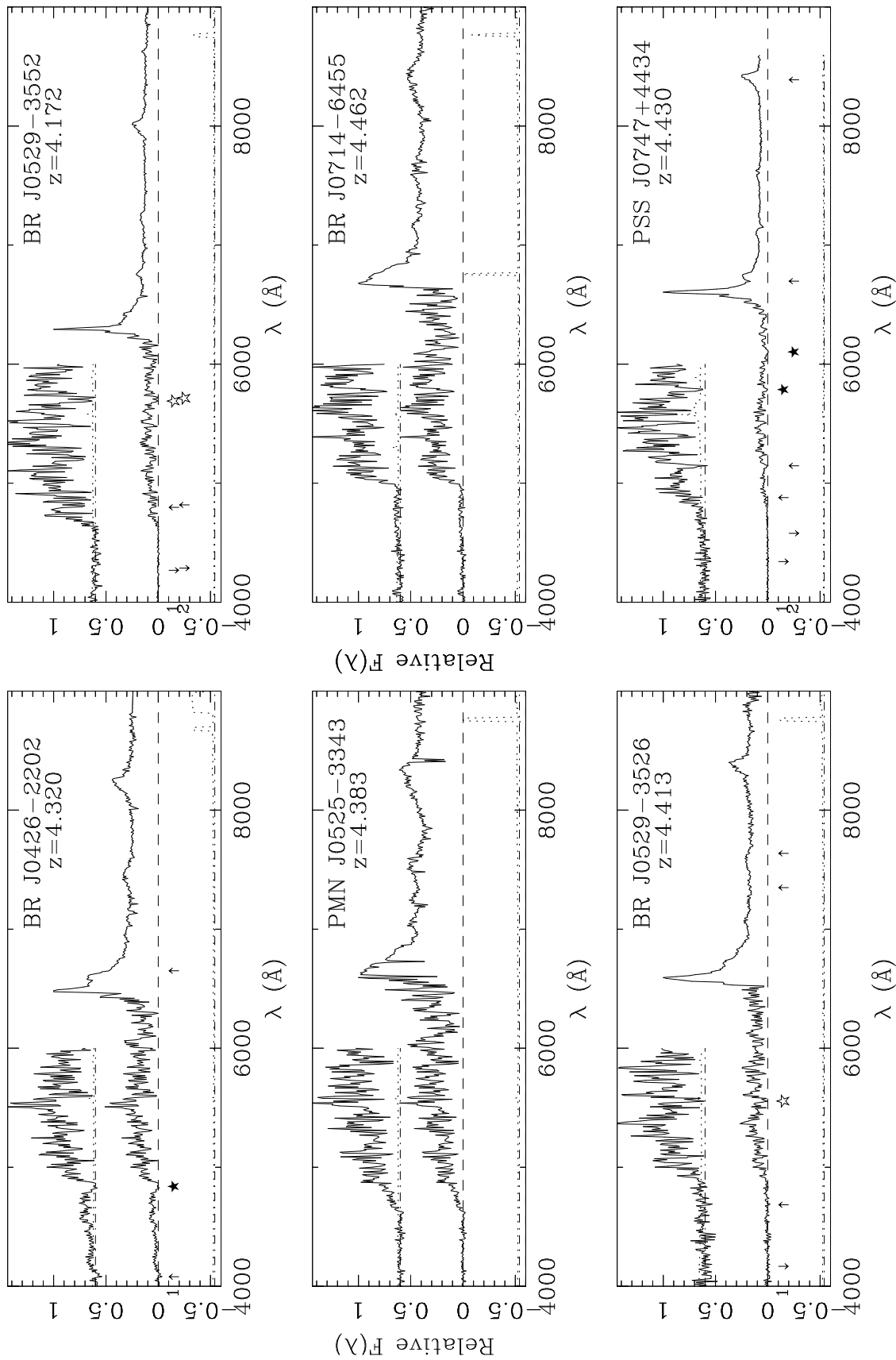
FIG. 1.— Spectra of all the observed quasars. The error arrays are plotted as dotted lines, offset below the spectra for clarity. In the upper left-hand corner, the blue region of the spectra are magnified to make the Lyman-limit systems and damped Ly α candidate absorbers easier to see. Damped Ly α candidate absorbers are marked below their positions as solid stars if they have estimated column densities $N_{\text{HI}} \geq 2 \times 10^{20}$ atoms cm $^{-2}$, and as open stars if they have estimated column densities lower than this threshold, but greater than 5×10^{19} atoms cm $^{-2}$. To the right of the stars marking the DLA are the detected metal lines that are associated with this absorber. To the left of the stars are an upward arrow marking the position of Ly β at the DLA redshift and a downward arrow marking the wavelength of the Lyman-limit that would be associated with this DLA.

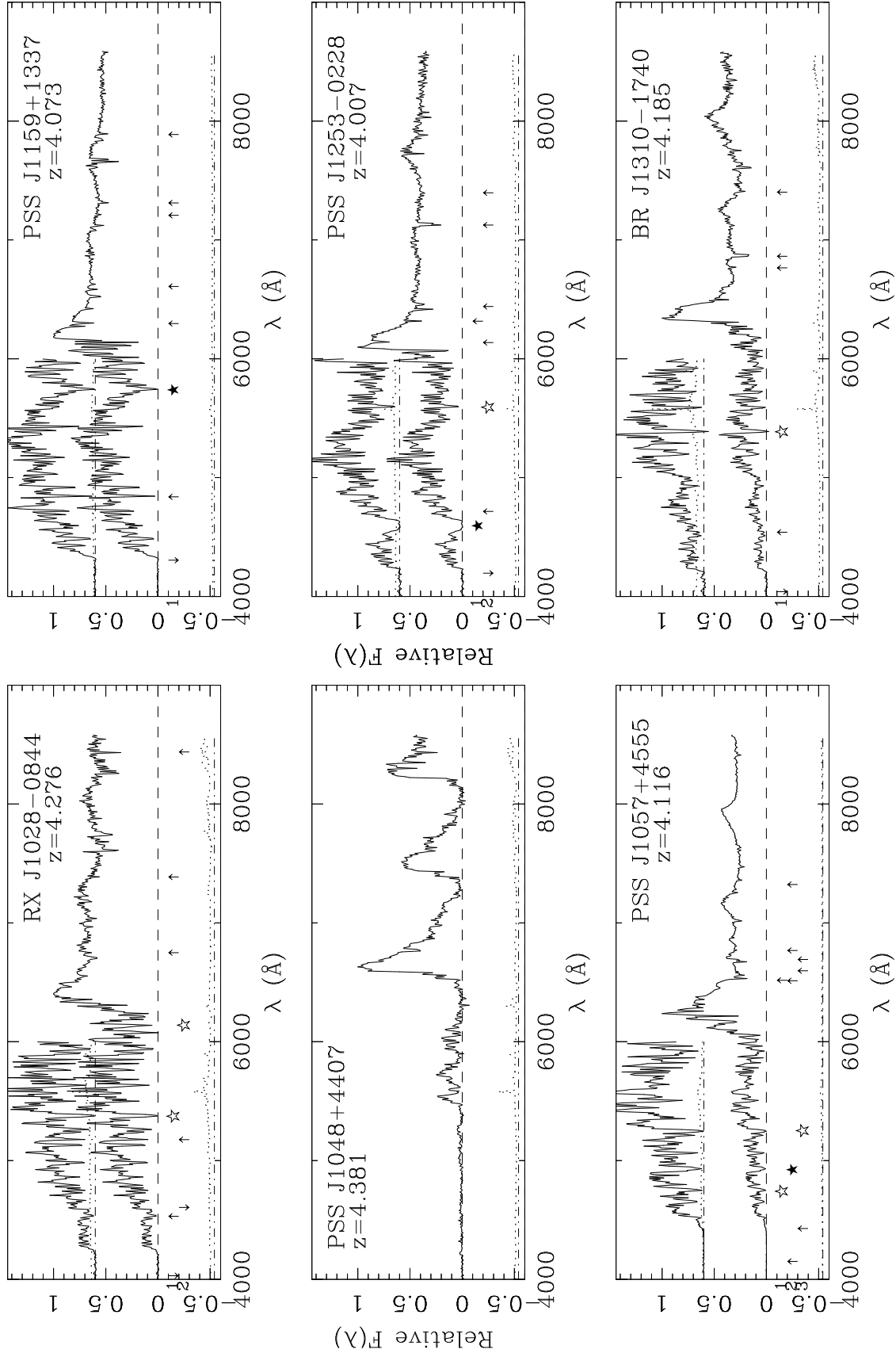
FIG. 1.— *continued*

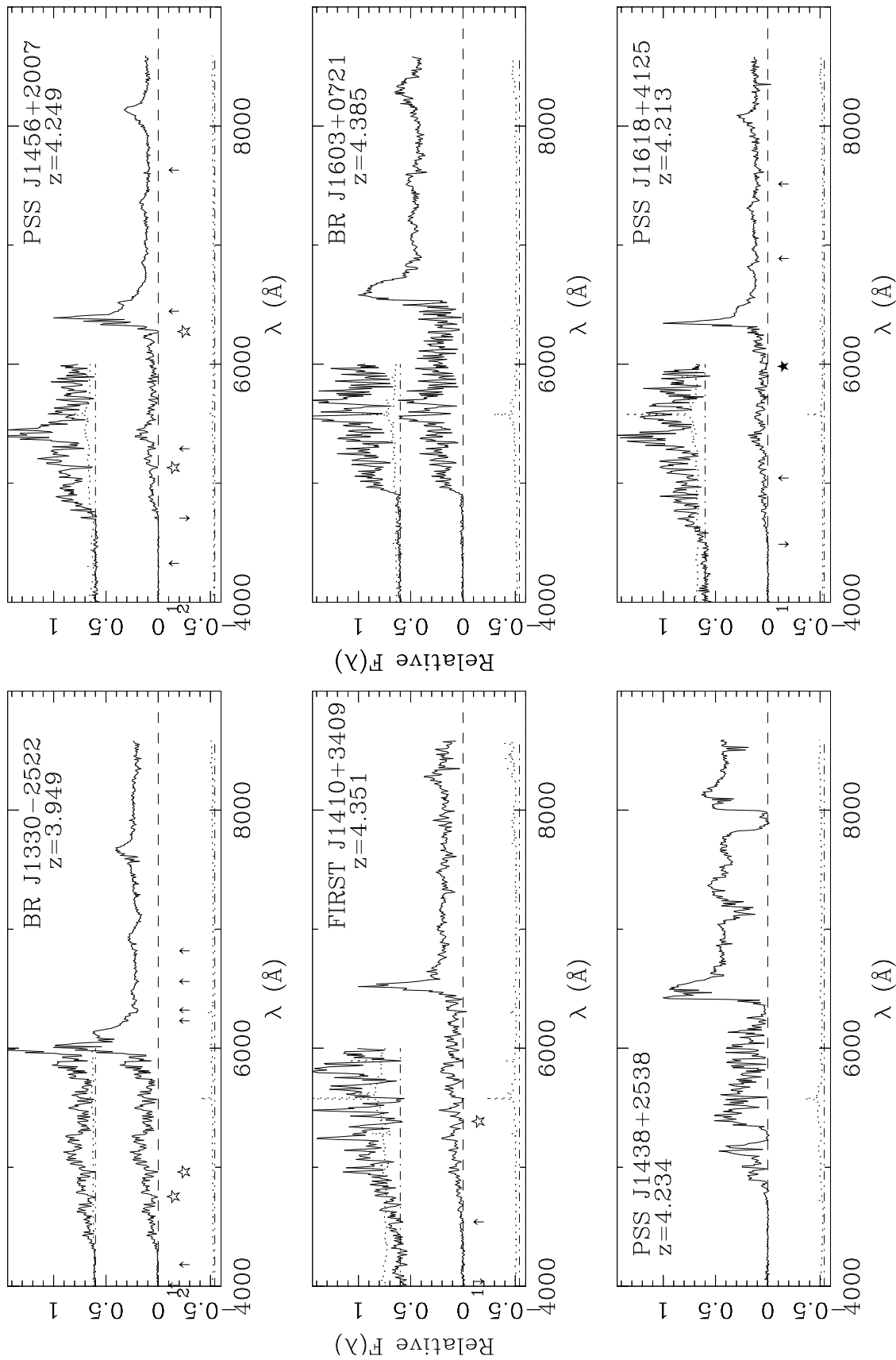
FIG. 1.— *continued*

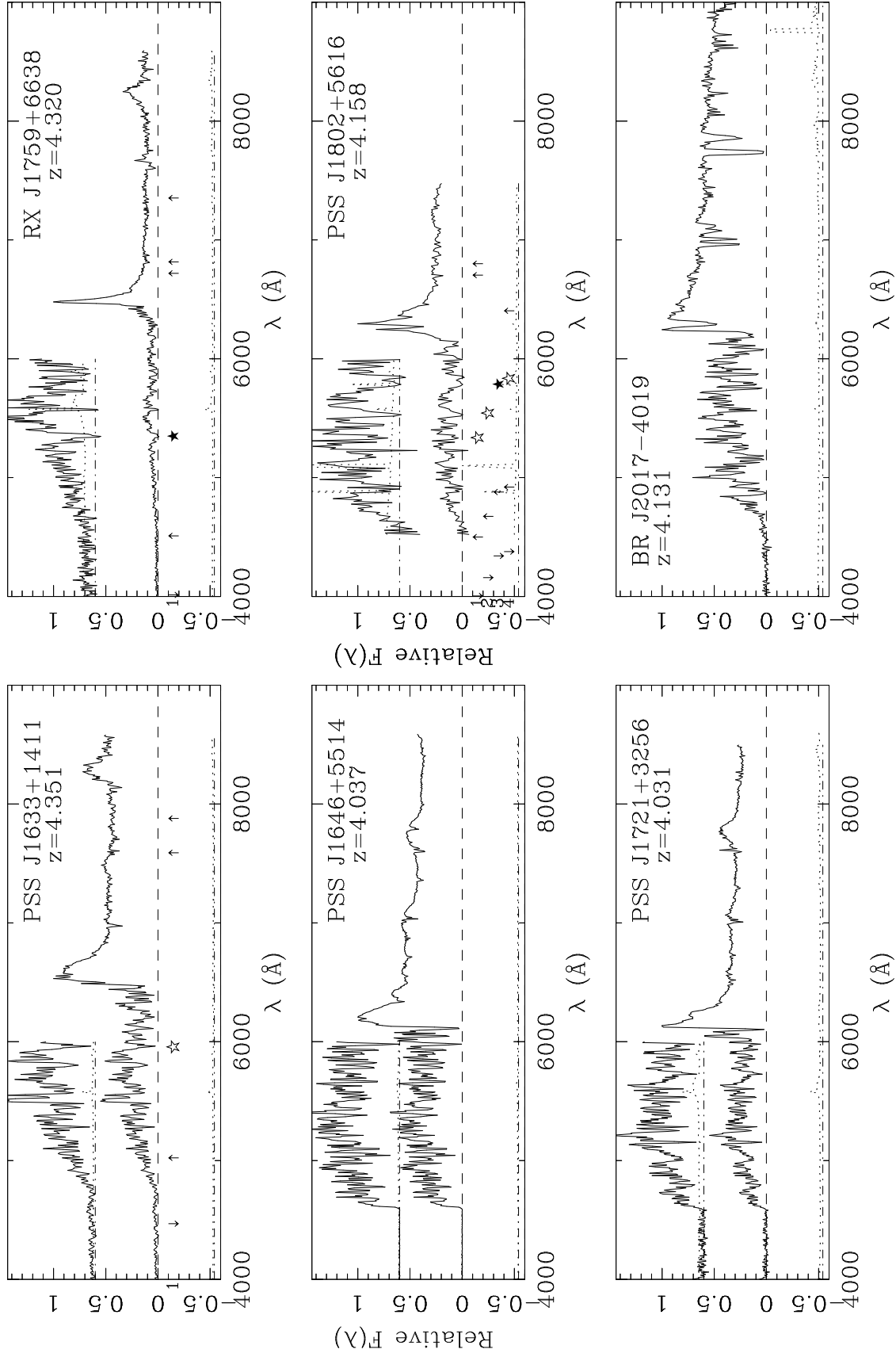
FIG. 1.— *continued*

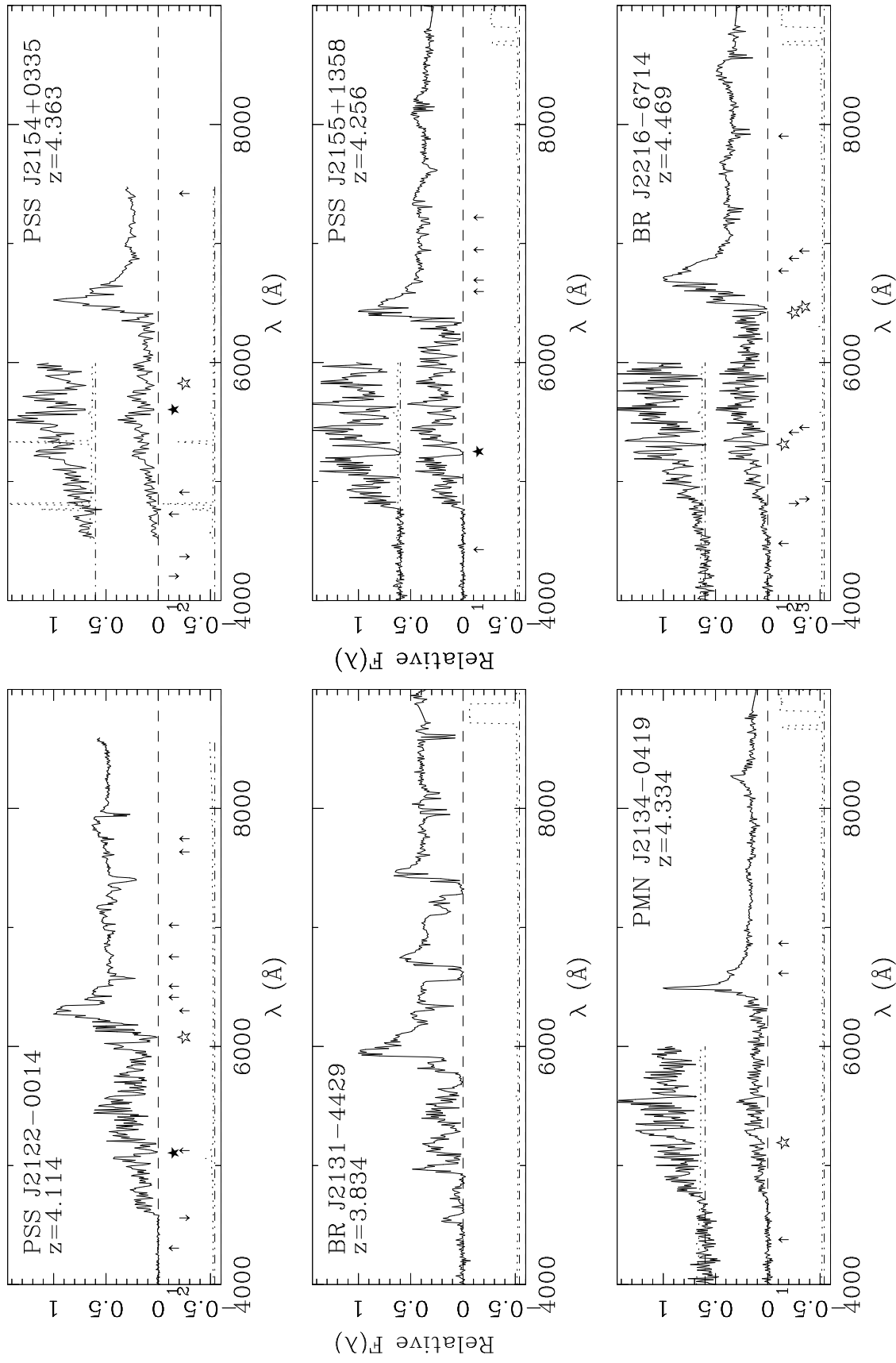
FIG. 1.— *continued*

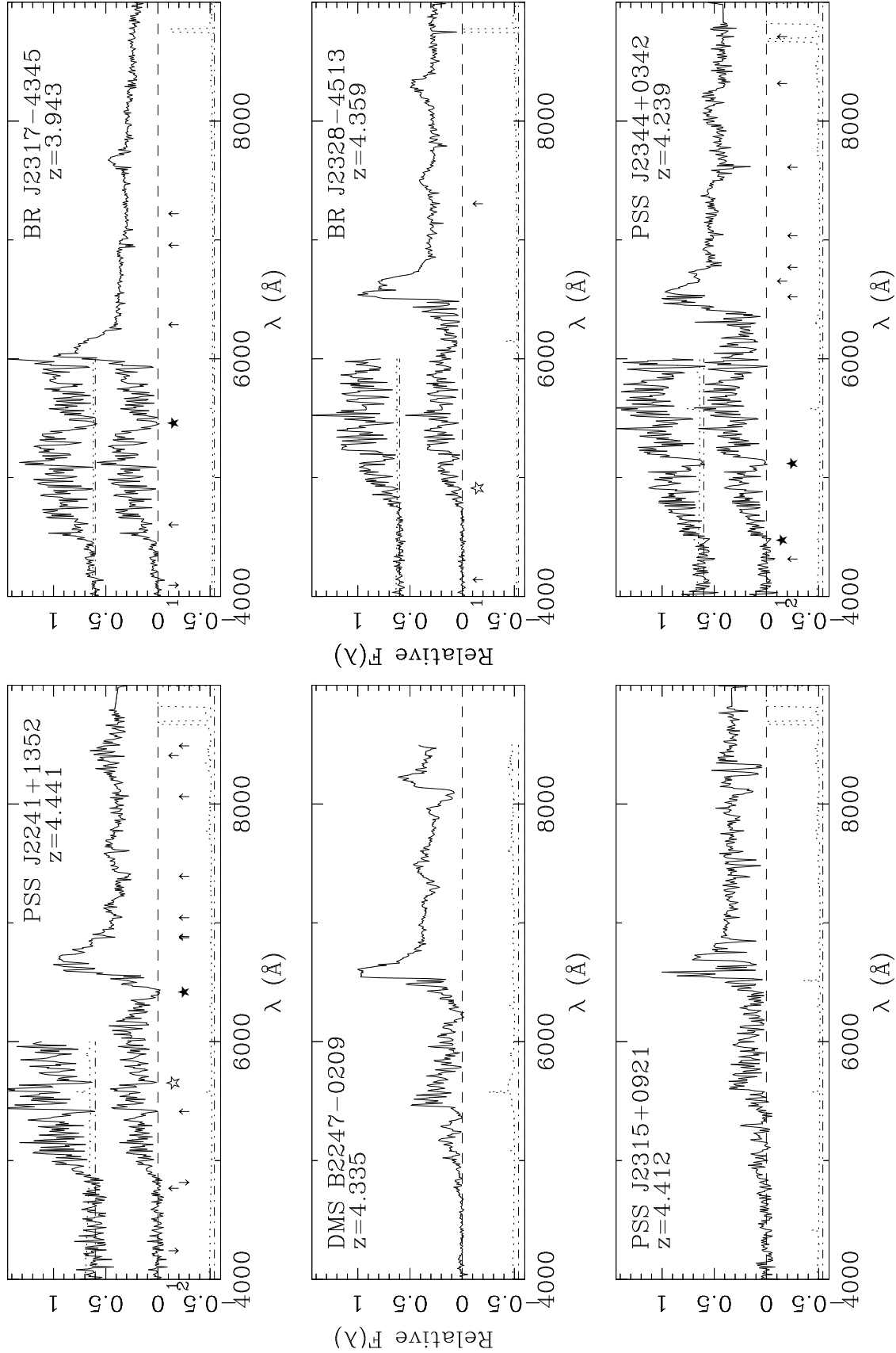
FIG. 1.— *continued*

FIG. 1.— *continued*

FIG. 1.— *continued*

FIG. 1.— *continued*

FIG. 1.— *continued*

FIG. 1.— *continued*

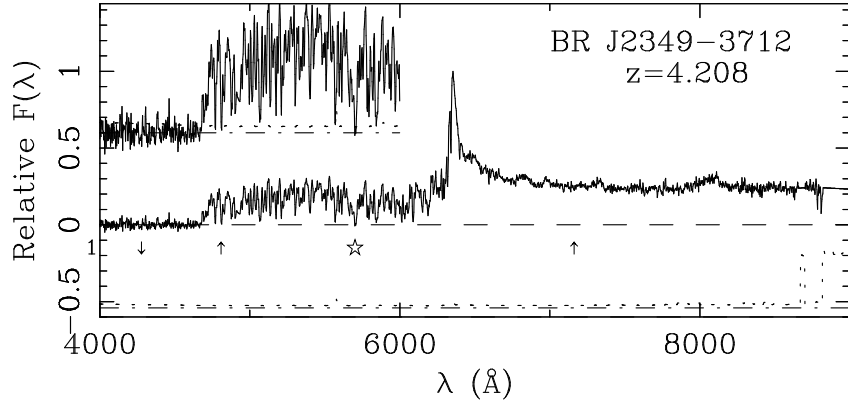
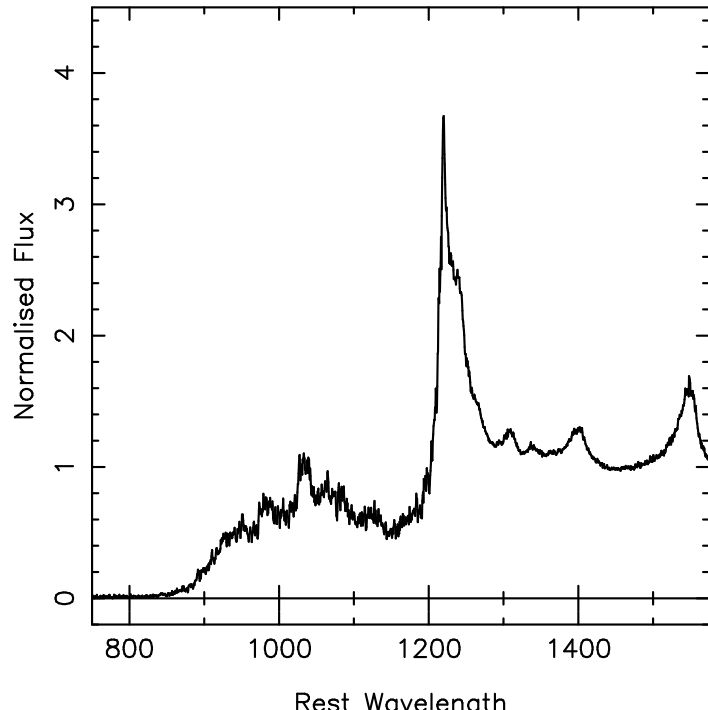
FIG. 1.— *continued*

FIG. 2.— Median composite spectrum. This is constructed by correcting each of the non-BAL spectra with enough wavelength coverage to rest frame and normalizing the flux over a region free of emission features (1420–1470 Å).

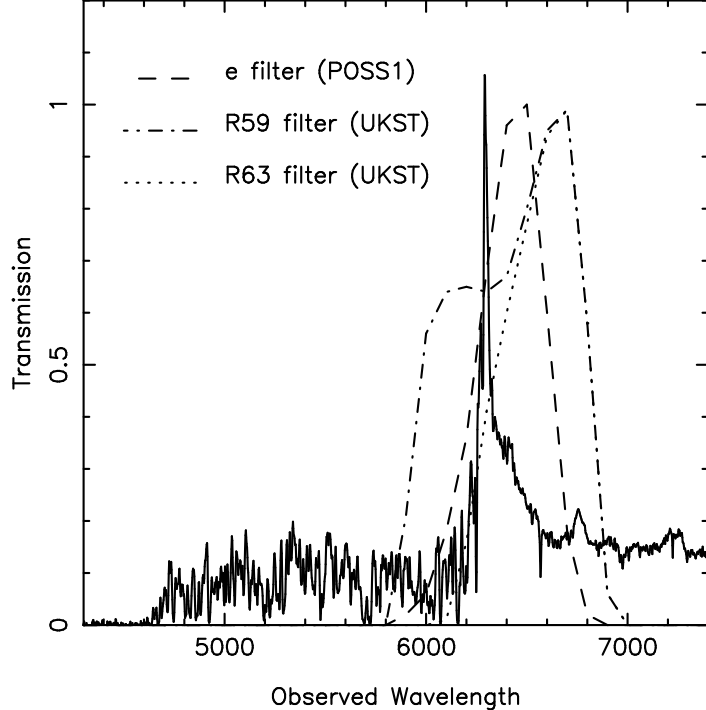


FIG. 3.— Filters used in various surveys. The R filters used for the photographic plates scanned with the APM facility are overplotted on the spectrum of $z=4.172$ BR J0529–3552. The “e” filter was used for the POSS1 survey and the “R59” (R) and “R63” (OR) were used for the UKST survey.

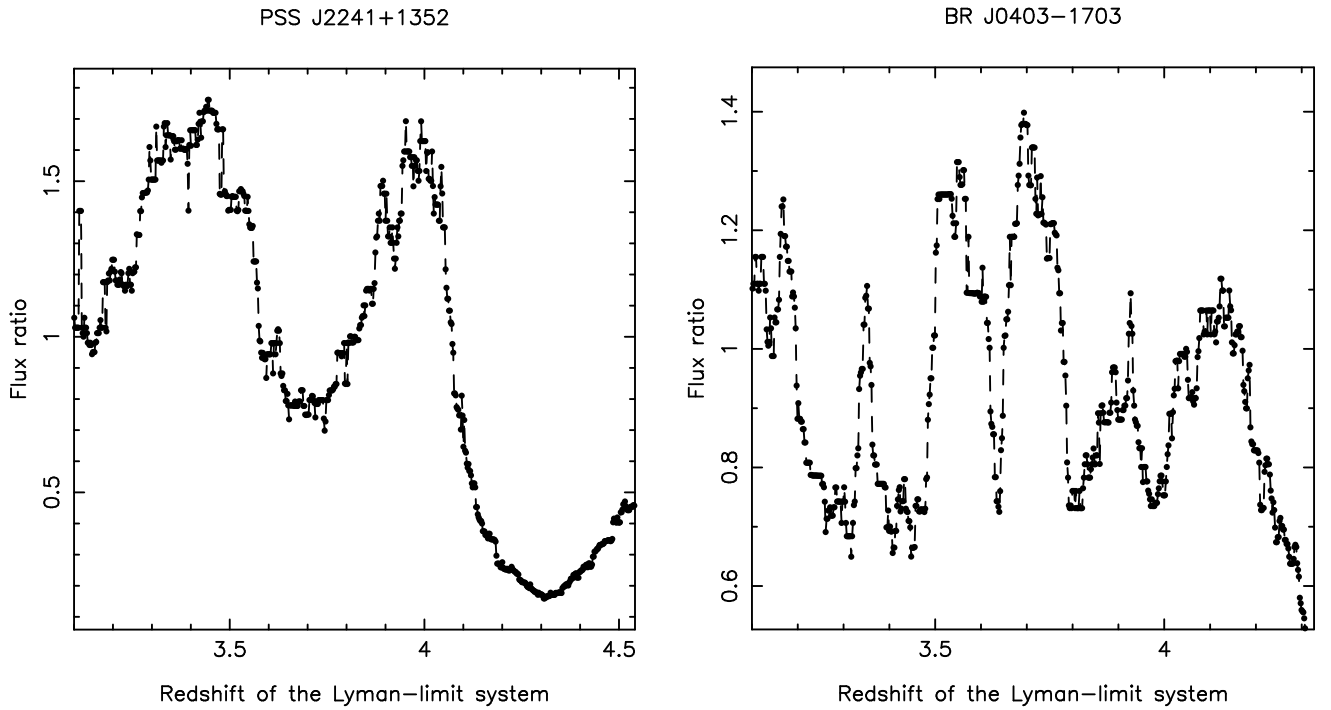


FIG. 4.— LLS detection. Examples of flux ratio above and below the putative Lyman-limit system redshifts. The plot for quasar PSS J2241+1352 (left panel) indicates a LLS with redshift $z = 4.31$ while the plot for quasar BR J0403–1703 (right panel) does not show the presence of a LLS.

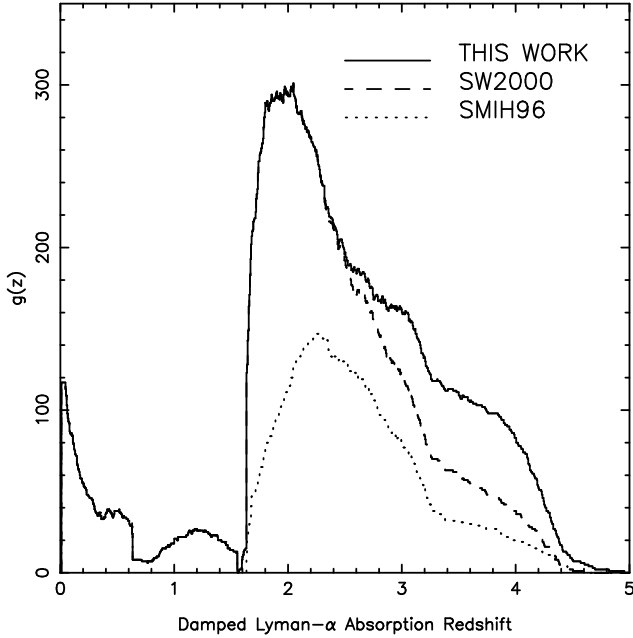


FIG. 5.— Survey sensitivity function. The $g(z)$ function shows the cumulative number of lines of sight along which a DLA system could be detected if there was one. SW00 and SMIH96 are surveys undertaken by Storrie-Lombardi & Wolfe 2000 and Storrie-Lombardi et al. 1996b, respectively. Our new observations more than doubles the redshift path surveyed at $z \geq 3.5$.

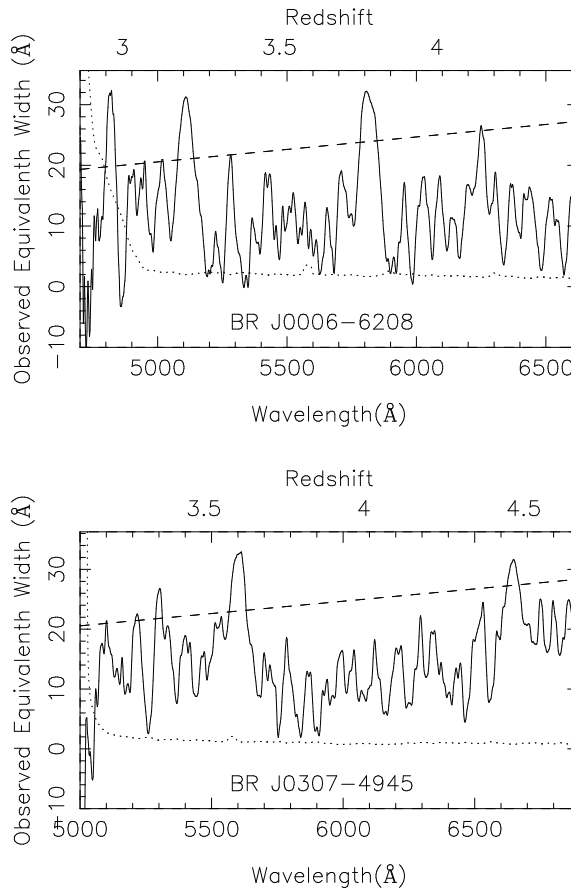


FIG. 6.— DLA detection. The figure shows two examples of the output from the algorithm that detects damped Ly α absorption candidates. The spectrum equivalent width bins are shown as a solid line, the error equivalent width bins are shown as a dotted line, and the dashed line shows the observed equivalent width of a 5 \AA rest equivalent width line at the redshifts shown along the top axis. The lower axis shows the wavelength scale. The minimum redshift (z_{min} in table 5) to which we can survey for damped candidates is determined by the point where the error line (dotted) crosses the 5 \AA rest equivalent width threshold (dashed line). The places where the spectrum array (solid line) goes above the dashed line threshold are the wavelengths at which we measure the aequivalent width of the lines in the original spectrum. The upper panel shows four potential absorbers in BR J0006-6208 and the lower panel shows 5 potential absorbers in BR J0307-4945.

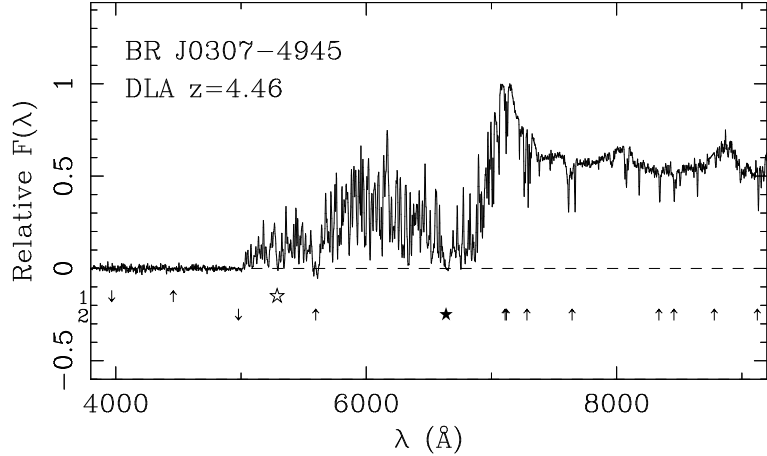


FIG. 7.— Example of DLA candidates. The spectrum of quasar BR J0307–4945 with DLA candidates marked at $z=4.46$ and $z=3.35$ is shown. The $z=4.46$ absorber is the highest redshift damped absorber currently detected. The notations are as in Figure 1. Many metal lines are observed at $z=4.46$ but no metals are detected at $z=3.35$. The higher redshift DLA has been studied in detail with higher-resolution observations undertaken with the UVES spectrograph (Dessauges-Zavadsky et al. 2000).